

Invisible decays of axion-like particles: constraints and prospects

Luc Darmé,^{1*} Federica Giacchino,^{1†} Enrico Nardi,^{1‡}
Mauro Raggi^{2§}

¹ *Istituto Nazionale di Fisica Nucleare, Laboratori Nazionali di Frascati, C.P. 13, 00044
Frascati, Italy*

² *Dipartimento di Fisica, Università di Roma La Sapienza and INFN, Sezione di Roma,
I-00185 Rome, Italy*

Abstract

Axion-like particles (ALPs) can provide a portal to new states of a dark sector. We study the phenomenology of this portal when the ALP mainly decays invisibly, while its interaction with the standard model sector proceeds essentially via its coupling to electrons and/or photons. We reanalyse existing limits from various collider and beam dump experiments, including in particular ALP production via electron/positron interactions, in addition to the usual production through ALP-photon coupling. We further discuss the interplay between these limits and the intriguing possibility of explaining simultaneously the muon and electron magnetic moment anomalies. Finally, we illustrate the prospects of ALP searches at the LNF positron fixed-target experiment PADME, and the future reach of an upgraded experimental setup.

*luc.darme@lnf.infn.it

†fgiacchi@lnf.infn.it

‡enrico.nardi@lnf.infn.it

§mauro.raggi@roma1.infn.it

Contents

1	Introduction	2
2	The axion-like particle portal	4
2.1	ALP effective Lagrangian	4
2.2	Astrophysical and cosmological constraints	6
2.3	ALPs production	9
3	Experimental searches for invisible ALPs	13
3.1	Limits from e^+e^- experiments	13
3.2	Limits from electron beam dump experiments	18
3.3	Simulation of ALP production in the PADME environment	20
3.4	Magnetic moment of light leptons	24
4	Results	26
4.1	Photo-philic or electro-philic ALP	26
4.2	Combined case	27
5	Conclusions	31

1 Introduction

The Standard Model of particle physics (SM) has proven to be an extremely accurate description of nature, predicting with high precision practically all of the observables measured experimentally during the last decades. Yet, its shortcomings are equally well-known, for instance the nature of dark matter, the strong CP problem, the neutrino masses or the origin of the SM flavour structure. Over the years, a large number of Beyond Standard Model (BSM) solutions to these issues have been introduced, but so far none has been experimentally validated. While many of these models rely on introducing new particles around the TeV scale, this is neither a requirement nor, in many cases, the simplest possibility. New, light but feebly interacting particles, singlets under the SM gauge group, can often provide the most straightforward solution.

One of the best motivated possibilities for such new light particles are pseudo-Nambu-Goldstone Bosons (pNGB) a , pseudoscalar particles coupled very feebly to ordinary matter and radiation which arise from an explicit breaking of an approximate global symmetry in the UV. Lagrangians involving these fields enjoy an approximate shift symmetry under which $a \rightarrow a + \text{const.}$, which implies that their interactions has to proceed via derivative terms. According to the nature of the quasi-exact global symmetry, the corresponding pNGB is often denoted by a specific name: familon [1], majoron [2,3], or axions [4–7]. More generally, light particles presenting the same types of derivative interactions are also motivated by various BSM theoretical scenarios, such as string theory [8,9], or by extensions to the SM designed to address specific SM issues such as the strong-CP problem [10,11] or the hierarchy problem [12].

From a bottom-up perspective, particles that enjoy the approximate shift symmetry mentioned above are often referred to as axion-like particles (ALPs).¹ While the

¹The name ‘ALP’ is inspired by the QCD axion, the difference being that ALPs are not required to solve the strong CP problem, in which case the mass and couplings of the ALP to fermions and

traditional mass range for such new particle typically extends in the extra-light, sub-eV region, the possibility of much more massive ALPs, in the MeV-GeV range, has received in recent years increasing attention (see. e.g. [13–20, 20–23] for recent works on ALPs coupled to photons/leptons). ALPs in this mass range have been invoked for example as a possible solution for both the muon and the electron magnetic moment anomalies [24–30] and, interestingly, viable solutions to these anomalies require both electromagnetic and leptonic ALP interactions. Last but not least, recent hints of the production of a 17 MeV boson in nuclear transitions [31–34] have also been interpreted in terms of an hypothetical new pseudo-scalar particle [23, 35, 36].

In this work we explore the possibility that an ALP acts as a portal towards a *dark sector* containing other invisible and light SM gauge singlets. Searches for such light and feebly interacting new particles can be carried out in experiments which trade a large energy scale for an increase in statistics and reduction in backgrounds [37, 38]. These so-called “high-intensity frontier” experiments have attracted a strong interest in recent years. Indeed, it has been known for a long time [39] that for interactions mediated by non-renormalisable operators of dimension $4 + n$ ($n = 1, \dots$), when the energy scales of the dark sector physics is accessible, fixed targets experiments may very well surpass colliders in sensitivity. Among various well established search strategies, a particularly powerful one is the search for missing energy in fixed target and beam-dump experiments, as it does not require any particular assumption on the underlying structure of the dark sector.

In this work we focus on updating the current limits derived from missing energy searches for an ALP-portal scenario, assuming that the ALP decays dominantly invisibly so that most of the existing limits from visible decays searches do not apply. Furthermore, in simplified ALP models generally used to put experimental limits, it is often assumed that ALPs have only one type of interaction, for instance a coupling to the photons. Here we work in the more general scenario of a MeV-scale ALP coupled to both photons and electrons. Our aim is to capture the general phenomenological aspects of an ALP with independent couplings to electron and photons, studying correlations between processes induced by the different interactions, with particular attention to possible changes in the existing limits. We cover all available missing-energy searches, including high-energy results from the DELPHI [40] as well as high-intensity frontier experiments as BaBar [41] and NA64 [42], and we also present projections for Belle-II [43]. As an illustration of the effect of adding an invisible decay channel for standard long-lived ALP beam dump searches, we further study the limit from the E137 experiment [44] as function of the ALP invisible branching ratio. We show that a large suppression of the visible decay rate is required to alleviate the constraints from this class of experiments. Finally, we discuss the prospects for exploring ALP models of this type at the Positron Annihilation into Dark Matter Experiment (PADME) [45, 46] located in the Laboratori Nazionali di Frascati (LNF) in Italy. As PADME is based on a fixed-target positron beam accelerator setup, its search techniques differ significantly from other missing mass experiments. Near future upgrades of this experiment (and of the serving beam infrastructure [47]) will be able to probe a parameter space region complementary to NA64. Our results also provide for the first time a complete assessment of the status of ALP based solutions to the $(g-2)_e$ and $(g-2)_\mu$ anomalies. Strikingly, we have found that ALPs with masses as low as a hundred MeV can still provide a viable solution, which lies within range of upcoming Belle-II results.

photons can be freely taken as independent parameters.

A minimal model realising the scenario of an ALP coupled to both photons and electrons will be presented in Section 2. Details about the astrophysical limits and ALP production channels at accelerators will be also presented in this Section. Section 3 is dedicated to a recast of existing limits from accelerator experiments, to present the details of our estimates for the electron and muon magnetic moments, and to a description of the possibilities for ALP searches at PADME. In Section 4 we present a comparison between different limits, and finally in Section 5 we draw our conclusions.

2 The axion-like particle portal

2.1 ALP effective Lagrangian

ALPs are naturally produced by the spontaneous breaking of a global symmetry at some large new physics scale Λ . We follow the effective field theory (EFT) approach and focus on the ALP interaction with leptons and photons after electroweak symmetry breaking. The effective Lagrangian thus contains

$$\mathcal{L} \subset \frac{1}{2}(\partial_\mu a)(\partial^\mu a) - \frac{1}{2}m_a^2 a^2 + \frac{1}{4}g_{a\gamma} a F_{\mu\nu} \tilde{F}^{\mu\nu} + \sum_{l=e,\mu,\tau} \frac{g_{al}}{2}(\partial_\mu a) \bar{l} \gamma^\mu \gamma^5 l , \quad (1)$$

where $\tilde{F}^{\mu\nu} = 1/2 \epsilon^{\mu\nu\alpha\beta} F_{\alpha\beta}$ with $\epsilon^{0123} = -1$. In the spirit of ALP phenomenology, we take the the mass m_a and the couplings $g_{a\gamma}$ and g_{al} to be independent parameters. The ALP interactions are described by dimension-5 operators and carry dimension of inverse mass (GeV^{-1}). The last term in Eq. (1) is often rewritten as $-ig_{al}m_l a \bar{l} \gamma_5 l$ after integrating by part and applying the equations of motion. However, in passing from the derivative to the pseudoscalar coupling an anomalous contribution to the ALP interaction with photons must be added to the second term in Eq. (1) [13]. In the rest of this work we will assume that the couplings to quarks and gluon are either absent, or negligible compared to $g_{a\gamma}$ and g_{ae} (see for instance [20] for a recent summary of the limits on those couplings).² As regards the couplings to the heavier τ and μ leptons, they would yield additional visible decays channels which in our analysis are not relevant. However, when we will briefly consider the prospects for the muon $g - 2$, $g_{a\mu}$ will clearly play a relevant role. We assume the presence of particles of a dark sector in which the ALP predominantly decays, therefore, besides the interactions in Eq. (1), the ALP couples derivatively to an axial-vector current involving dark sector states $\mathcal{J}_{5,D}^\mu$:

$$\mathcal{L} \supset \frac{g_{a\chi}}{2}(\partial_\mu a) \mathcal{J}_{5,D}^\mu . \quad (2)$$

For example, for a dark Dirac fermion χ one has $\mathcal{J}_{5,D}^\mu = \bar{\chi} \gamma^\mu \gamma^5 \chi$.

The decay widths into two-photons or into an electron-positron pair are given by

$$\Gamma_{\gamma\gamma} = \frac{g_{a\gamma}^2 m_a^3}{64\pi} \quad (3)$$

$$\Gamma_{e^+e^-} = \frac{g_{ae}^2 m_e^2 m_a}{8\pi} \sqrt{1 - \frac{4m_e^2}{m_a^2}} , \quad (4)$$

²We also assume that the $Z\gamma$ mixed coupling arising from the ALP interaction in an $SU(2)$ -preserving basis is negligible, corresponding to coupling the ALP to B and W vector boson with the same strength (see, e.g. [14]).

while the invisible decay width into a pair of dark Dirac fermions reads:

$$\Gamma_{\text{inv}} = \frac{g_{a\chi}^2}{8\pi} m_\chi^2 m_a \sqrt{1 - \frac{4m_\chi^2}{m_a^2}}. \quad (5)$$

Due to the m_a^3 scaling of the two-photon decay width, it is clear that one typically expects the photonic channel to dominate the visible decays at large ALP masses, except in the case of a significant hierarchy between the photon and the electron couplings. Let us define the visible decay rate of the ALP as $\Gamma_{\text{vis}} = \Gamma_{\gamma\gamma} + \Gamma_{e^+e^-}$. The main assumption in this work is dominance of the invisible decays, that is

$$\Gamma_{\text{inv}} \gg \Gamma_{\text{vis}} = \Gamma_{\gamma\gamma} + \Gamma_{e^+e^-}. \quad (6)$$

These partial decay rates have important implications for both visible and invisible decays. Indeed if the size of the detector (for example, the distance between the target and the calorimeter at fixed target experiments) is smaller than the decay length, long-lived particles can mimic an invisible decay event. The typical ALP decay length ℓ_a is given approximately by:

$$\ell_a \sim 0.1 \text{ m} \times \left(\frac{100 \text{ MeV}}{m_a} \right) \times \left[\left(\frac{g_{a\chi} m_\chi}{0.7 \cdot 10^{-6}} \right)^2 + \left(\frac{g_{a\gamma} m_a}{2 \cdot 10^{-6}} \right)^2 + \left(\frac{g_{ae} m_e}{0.7 \cdot 10^{-6}} \right)^2 \right]^{-1}. \quad (7)$$

where we have assumed $m_a \gg m_\chi, m_e$ and Dirac dark fermions as an example of a possible dark sector. From the above equation it is clear that invisible decays will dominate as long as:

$$g_{a\chi} m_\chi \gg g_{a\gamma} m_a, g_{ae} m_e. \quad (8)$$

Furthermore, detection in beam dump experiments searching for visible ALP decay will be severely restricted as long as the invisible decay length is too short, which could typically occur in the region of parameter space where $g_{a\chi} m_\chi \gg 10^{-5}$.

Let us note that in the case of a significant hierarchy between $g_{a\gamma}$ and g_{ae} , the subdominant coupling will receive important one-loop contributions generated by the leading one. Given that the experimental limit are typically much stronger for $g_{a\gamma}$, it is interesting to consider the electron one-loop contribution proportional to $g_{ae} \alpha_{\text{em}}$. Using the derivative ALP-electron interaction from Eq. (1) we have [13]:

$$\delta g_{a\gamma} = \frac{\alpha_{\text{em}} g_{ae}}{\pi} B_1 \left(\frac{4m_e^2}{m_a^2} \right), \quad (9)$$

where the scalar loop function B_1 is given by:

$$B_1(\tau) = 1 - \tau f(\tau)^2, \quad f(\tau) \equiv \begin{cases} \arcsin(1/\sqrt{\tau}) & , \tau \geq 1 \\ \left[\frac{i}{2} \log \frac{1+\sqrt{1-\tau}}{1-\sqrt{1-\tau}} + \frac{\pi}{2} \right] & , \tau < 1, \end{cases} \quad (10)$$

with $B_1(\tau) \rightarrow 1$ for $\tau \rightarrow 0$ and $B_1(\tau) \sim 1/(3\tau)$ for $\tau \gg 1$. For $m_a \gg m_e$ one obtains $\delta g_{a\gamma} \sim 0.001 g_{ae}$, and one can thus expect the decay into photons to dominate over the decays into electrons as long as $m_a \gtrsim 1 \text{ GeV}$. Note that, if the correction to the ALP-photon coupling is computed using instead the non-derivative coupling to the pseudoscalar electron density, one would find a result proportional to $B_1(\tau) - 1$ which

in the limit of large fermion mass $\tau \gg 1$ does not decouple. However, as was pointed out in [13], the surviving -1 precisely cancels the anomalous contribution that, as was mentioned below Eq. (1), had to be added to the ALP-photon interaction term when passing from the derivative of the axial-vector current to the pseudoscalar electron density. In the rest of this work, we will assume the coupling $g_{a\gamma}$ to be a completely free parameter, keeping in mind that a ratio $g_{a\gamma}/g_{ae}$ smaller than ~ 0.001 is not completely natural, and requires a certain level of tuning of the relevant parameters.

2.2 Astrophysical and cosmological constraints

Relic density and CMB. An ALP decay channel into invisible particles of a dark sector, and the corresponding suppression of the branching ratios for visible decays, can relax the limits from laboratory experiments, as well as from the cosmological imprint in the cosmic microwave background (CMB) that could arise from late time decays (see e.g. the recent study in ref. [48]). However, the presence of new, light, and feebly coupled degrees of freedom has other preeminent consequences in cosmology and especially in astrophysics.

If stable, dark sector particles may constitute all or part of the Dark Matter (DM) content of the universe, a possibility has been studied in the last decade by various groups. However, it is relatively hard to suppress the relic density to an acceptable level in vanilla freeze-out scenarios that exploit a higher-dimensional portal (early studies include refs. [49, 50]). Moreover, an additional difficulty is that of evading CMB limits on late-time annihilating DM [51]. Indeed, a DM candidate with mass below ~ 10 GeV would still keep annihilating at the time of matter-radiation decoupling, and would produce sizeable distortions of the CMB spectral shape [52].³ Nevertheless, a number of ways out from these difficulties have been put forth throughout the years. One possibility is to add a secluded annihilation channel via a renormalizable operator to fix the correct relic density, and then select a type of final states that will decay sufficiently fast in order to avoid all BBN and CMB constraints [54–57]). Another possibility, that was sketched for example in ref. [58], is to use the entropy dilution from the decay of heavier relics to suppress the large relic density of keV-scale DM left over by inefficient annihilation via the higher-dimension portal. In this case a complete cosmological model should also include the dependency on the reheating temperature for the production of the heavy relics, which is also subject to specific constraints. More exotic cosmological scenarios, such as a late time phase transition, can additionally have strong effects on the resulting relic density (see e.g. [59, 60] and related literature). With a set of *ad hoc* assumptions the minimal scenario outlined below Eq. (2) with the dimension five ALP portal and only one dark fermion χ can also be rendered viable. For instance, Ref. [14] assumed a resonance setup where $2m_\chi \lesssim m_a$ boosts the annihilation rate at earlier times, while later on at the BBN and CMB epochs the resonant annihilation channel is quenched because of the lower temperatures. In such case the proper relic density can be obtained for $g_{a\gamma}$ couplings as low as 10^{-5} GeV $^{-1}$. In this work, given that we do not specify the detailed structure of the dark sector, we will simply assume that a mechanism exists that allows to escape the constraints from DM overabundance, and possibly can fix the relic density to what is required to explain the DM.

³Indirect detection limits, in particular from Fermi-LAT [53], also constrain the mass region above ~ 200 MeV.

SN1987 limits. The duration of the neutrino burst from the supernova SN1987A provides to this date one of the strongest limit on several types of light new particles. In fact, particles with mass up to several tens of MeV could be efficiently produced in the collapsed core of a SN, and if they can freely escape, they would increase the cooling rate of the SN core and thus shorten the duration of the neutrino burst. However, if the interactions of these new particles with the surrounding medium are not sufficiently feeble, they would remain trapped in the core of the proto-neutron star and would not contribute to the cooling [61, 62]. According to the recent study in Ref. [63] this would for example happen for ALP-photon couplings $g_{a\gamma} \gtrsim 10^{-6} - 10^{-5}$ while, to the best of our knowledge, no analogous limit has been derived for the case of a purely electrophilic ALP (this might be due to the fact that ALP-electron couplings are usually considered in combination with ALP-quark interactions, which are expected to dominate because of the induced couplings of the ALP to the nucleons). The above result for $g_{a\gamma}$ implies that for practically the whole parameter space relevant for this work, the ALP will remain trapped and thus SN1987A does not provide useful constraints. Only in the lowest part of parameter space ($g_{a\gamma} \lesssim 10^{-5} \text{ GeV}^{-1}$) trapping via ALP-photon interaction might be avoided. However, due to the intrinsic difficulty in pinning down the precise boundary between the trapping and free streaming regimes, it is safer to assume that also this region remains at least marginally compatible with the SN bound. The limits on the ALP couplings to SM particles, however, are of little importance in our case, since the decay/inverse-decay process $a \leftrightarrow \chi\bar{\chi}$ changes dramatically the discussion. In fact, as was noted in [14], even when the ALP is trapped because of sizeable $g_{a\gamma}$ or g_{ae} couplings, the dark fermions χ might still escape and drain energy from the SN core, because χ -trapping is much more difficult to achieve due to the dimension-5 nature of the ALP portal. However, Ref. [14] only considered the scattering processes $\bar{\chi}\chi \leftrightarrow \text{SM SM}$ for which the rates are heavily suppressed. We find instead that in the regime in which the ALP is trapped, χ interactions with on-shell ALPs give the dominant contribution to reduce the χ mean-free-path and to keep them trapped.

The SN limits for light dark matter are typically derived in two-steps. First, one estimates the luminosity \mathcal{L}_χ of the black body emission of fermions from a χ -sphere of radius R_χ defined, in analogy to the usual neutrino-sphere, as the boundary surface between the trapping and free streaming regimes. For a Dirac fermion χ we have (see e.g. [64]):

$$\mathcal{L}_\chi = \frac{g_\chi}{2\pi} \int_{m_\chi}^{\infty} dE \frac{E(E^2 - m^2)}{e^{E/T(R_\chi)} + 1} \xrightarrow{m_\chi \ll T} \frac{7g\pi^3}{240} R_\chi^2 T(R_\chi)^4, \quad (11)$$

where T is the temperature and g the number of degrees of freedom of the emitted particle ($g = 4$ for a Dirac fermion). Using the core profile from [65] and the neutrino luminosity $\mathcal{L}_\nu \sim 3 \cdot 10^{52} \text{ erg s}^{-1}$ [62, 65] we obtain that the typical radius for which $\mathcal{L}_\chi \lesssim \mathcal{L}_\nu$ is $R_\chi \sim 20 \text{ km}$ for m_χ around 10 MeV. The second step is that of estimating R_χ which, as anticipated, is mainly determined by the inverse-decay process $\chi\bar{\chi} \rightarrow a$, as function of $g_{a\chi}$. Using the narrow width approximation ($\Gamma_a \ll m_a$) which is always very accurate for the weakly interacting χ , the relevant cross-section reads:

$$\sigma_{res} = \frac{\pi g_{a\chi}^2 m_\chi^2}{2\sqrt{1 - 4m_\chi^2/m_a^2}} \delta(s - m_a^2) \equiv \tilde{\sigma}_{res} \delta(s - m_a^2). \quad (12)$$

The number of interactions a χ particle suffers along an outward trajectory from R_χ

is:

$$N_{int} = \int_{R_\chi}^{R_{far}} dr \left[\frac{g_\chi}{n_\chi(T_{R_\chi})} \int d^3\Pi_\chi d^3\Pi_{\bar{\chi}} f_\chi(T_{R_\chi}) f_{\bar{\chi}}(T) 4E_\chi E_{\bar{\chi}} \sigma_{res} \right], \quad (13)$$

where $d^3\Pi$ is the standard Lorentz-invariant phase-space, R_χ is the radius of the dark sector sphere determined above, $f_\chi = (\exp(m_\chi/T) + 1)^{-1}$ is the Fermi-Dirac statistical distribution, and $R_{far} \sim 100$ km corresponds to the outer layers of the proto-neutron star, out of which the profiles are not accurate. Altogether, Eq. (13) is simply the thermal average (taken at T_{R_χ}) of the number of interactions that a fermion χ emitted from R_χ has with the surrounding halo of $\bar{\chi}$'s to resonantly produce an ALP. Given the simple form of σ_{res} and the symmetric structure in $\bar{\chi}$ and χ , the integral can be evaluated straightforwardly. Using standard integration techniques from the dark matter playbook (see e.g. the nice Appendices in [66]) we have

$$d^3\Pi_\chi d^3\Pi_{\bar{\chi}} = \frac{|p_\chi| |p_{\bar{\chi}}|}{32\pi^4} dE_\chi dE_{\bar{\chi}} d\cos\theta, \quad (14)$$

where θ is the angle between χ and $\bar{\chi}$, and $|p_\chi|, |p_{\bar{\chi}}|$ their three-momenta. Using also

$$s = 2m_\chi + 2(E_\chi E_{\bar{\chi}} - |p_\chi| |p_{\bar{\chi}}| \cos\theta), \quad (15)$$

and absorbing the angular integration by means of the delta function in Eq. (12), we obtain the simple expression:

$$N_{int} = \int_{R_\chi}^{R_{far}} dr \left[\frac{g_\chi}{n_\chi} \int_{m_\chi}^{\infty} \int_{m_\chi}^{\infty} dE_\chi dE_{\bar{\chi}} \left(\frac{E_\chi E_{\bar{\chi}}}{(e^{E/T(r)} + 1)(e^{E/T(R_\chi)} + 1)} \Theta(E_1, E_2) \right) \frac{\tilde{\sigma}_{res}}{16\pi^4} \right], \quad (16)$$

where $\Theta(E_\chi, E_{\bar{\chi}}) = 1$ in the resonance region defined by $s = m_a^2$, and 0 outside. Requiring at least one inverse-annihilation $N_{int} \geq 1$, and taking as an example $m_\chi = m_a/3$, leads to the trapping limit on the χ -ALP coupling

$$g_{a\chi} m_\chi \gtrsim 10^{-6}, \quad (17)$$

that holds for m_χ between $\sim 5 - 50$ MeV.⁴ Although Eq. (17) is just an order of magnitude estimate, that moreover has been derived for the specific case of a DM Dirac fermion, it clearly shows that trapping can be achieved with reasonable dark sector couplings (typically of the order of the experimental limit on g_{ae} , which is consistent with our initial assumption of ALP decays dominated by invisible channels). We can then conclude that in our case the ALP limits from SN1987A cannot be applied.

Altogether, we conclude that the limits from SN1987 cooling can be escaped by trapping the light dark matter in the proto-neutron star via its resonant annihilation into ALP. In the following we will thus simply assume that the dark coupling $g_{a\chi}$ is large enough to trap χ and will focus instead on the collider signatures directly. Note that since the dark matter still does travel before annihilating, one should more rigorously

⁴An alternative approach is that of estimating directly the mean free path for a particle χ of energy $E_\chi \gtrsim m_a/2$ and of mass in the tens of MeV range, emitted from the χ -sphere R_χ , and to require a mean free path of the order of 1 km. Following this procedure we have found a value of $g_{a\chi} m_\chi$ of the same order of magnitude than in Eq. (17).

consider the energy flux mediated by this process, using quantities like the Rosseland mean opacity [62]. In that case, the precise structure of the dark sector should be fleshed out, in particular if it contains more than one field. Nonetheless, Eq. (17) is several orders of magnitude below what will be typically required to maintain an invisible ALP while having $g_{ae}, g_{a\gamma}$ around the state of the art limits from laboratory based experiments, so we still expect the later constraint to the dominate.

As a final comment, recent works [63, 67] have further pointed to the possible importance of the dark sector particles in the description of the actual supernova explosion. Deriving actual constraints from such considerations would however require an actual simulation of the supernova including the presence of a dark sector.

2.3 ALPs production

ALPs can be produced through many processes in lepton-based experiments. Since we focus mostly on missing energy searches, we will typically require an additional photon final state to trigger on the events. The main channels in lepton beam accelerators are shown in Fig. 1. For positron beam experiments or e^+e^- colliders, the dominant processes are annihilation in the s or t-channel $e^+ + e^- \rightarrow \gamma + a$ (Fig. 1a and 1b), the former depending on the electron coupling g_{ae} and the later on the ALP-photon coupling $g_{a\gamma}$. In electron-beam experiments, the dominant processes are either ALP direct bremsstrahlung production via the g_{ae} coupling shown in Fig. 1c, or the successive processes, $e^-Z \rightarrow e^-Z\gamma$ and $\gamma Z \rightarrow \gamma Za$ for the coupling $g_{a\gamma}$, shown in Fig. 1d. While we will consider only the above production processes in this work, it is worth noting ALP probes via Primakoff process or Compton-like channels could be of importance for \lesssim MeV masses [68].

Positron-electron annihilation processes Focusing first on the associated annihilation processes – relevant for positron beam and e^+e^- experiments – we find that the total annihilation cross-section in the laboratory frame is given by:

$$\begin{aligned} \sigma = \sigma_{a\gamma} + \sigma_{ae} + \sigma_{int} &= \alpha_{\text{em}} g_{a\gamma}^2 \frac{(s + 2m_e^2)(s - m_a^2)^3}{24\beta s^4} \\ &+ \alpha_{\text{em}} g_{ae}^2 m_e^2 \frac{-2m_a^2\beta s + (s^2 + m_a^4 - 4m_a^2 m_e^2) \log \frac{1+\beta}{1-\beta}}{2(s - m_a^2)s^2\beta^2} \\ &+ \alpha_{\text{em}} g_{a\gamma} g_{ae} m_e^2 \frac{(s - m_a^2)^2}{2\beta^2 s^3} \log \frac{1 + \beta}{1 - \beta} \end{aligned} \quad (18)$$

where $\alpha_{\text{em}} = e^2/(4\pi)$ is the standard electromagnetic fine structure constant, m_e the electron mass, $\beta = \sqrt{1 - \frac{4m_e^2}{s}}$ and \sqrt{s} is the center-of-mass energy. In Eq. (18), $\sigma_{a\gamma}$ refers to the photon-mediated cross-section, σ_{ae} to the electron-mediated one and σ_{int} refers to the interference between these two channels.

The plots in Fig. 2 show the different behaviours of $\sigma_{a\gamma}$ and σ_{ae} as a function of the ALP mass m_a for various beam energies. Interestingly, both processes have a starkly different behaviours, due to the presence of a resonant enhancement in the soft-photon limit in the t/u-channel process of Fig. 1a. On the other hand, both $g_{a\gamma}$ and g_{ae} production rates are roughly of the same order when one has:

$$g_{a\gamma} \sim \frac{g_{ae} m_e}{\sqrt{s}}. \quad (19)$$

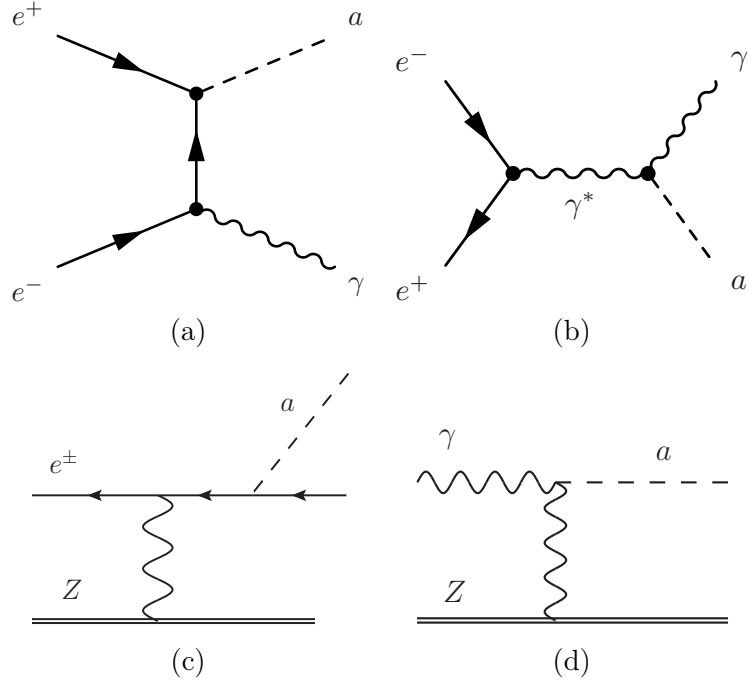


Figure 1: Feynman diagrams for ALP production: (a) t-channel annihilation process $e^+e^- \rightarrow \gamma + a$; (b) s-channel annihilation process $e^+e^- \rightarrow \gamma + a$; (c) Bremsstrahlung production on a target nucleus of atomic number Z , $e^\pm \rightarrow Z + e^\pm + a$ and (d) Primakoff production from secondary photon $\gamma + Z \rightarrow Z + a$.

This relation underlines much of the phenomenology of the next sections: photon-induced production mechanisms are relevant for large center-of-mass energies, while the converse is true for electron-induced processes. In particular, the associated production presents a resonant enhancement when $m_a \sim \sqrt{s}$. Altogether, it is clear that high-precision but low-energy positron-based experiment should be more efficient in constraining the fermionic coupling since they can rely on resonant production to significantly enhance the production rate.

Interestingly, the interference term in Eq. (18) presents the downsides of both production mechanisms, and is subdominant for all the parameter space we probed. Indeed, considering the “maximum interference” scenario where $g_{a\gamma} = \frac{g_{ae}m_e}{\sqrt{s}}$, we see that it does not present resonant enhancement when $m_a \sim \sqrt{s}$, and further scales as m_e/\sqrt{s} in the large $\sqrt{s} \gg m_a$ limit.

Bremsstrahlung process In a second time, let us consider the production for electron beam experiments. In this case, ALP production relies on interactions with the electromagnetic field sourced by the nuclei. Concerning the case of an electron/ALP bremsstrahlung the underlying physics has been known for several decades [69]. One can describe the actual effective $NN\gamma$ vertex via the nuclear and atomic form factors $G_2(t)$, with $G_2(t) = G_2^{el} + G_2^{in}$. Defining t the virtuality (i.e. squared momentum) of the photon

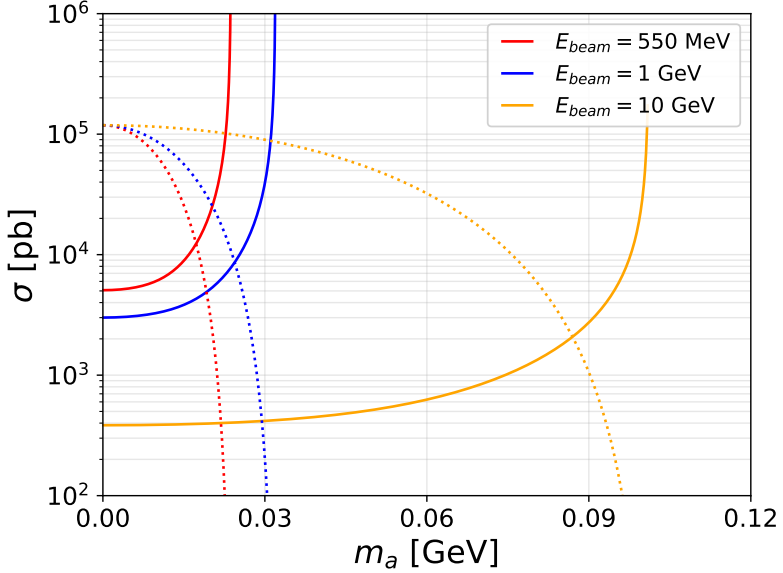


Figure 2: Annihilation cross-section as a function of ALP mass m_a for several values of E_{beam} ($= 0.55, 1, 10$ GeV) of photon mediator exchanged in s-channel diagram (dotted line) and electron mediator exchanged in t- and u-channel diagrams (continues line). The cross-section are given for $g_{a\gamma} = 1 \text{ GeV}^{-1}$ and $g_{ae} = 1 \text{ GeV}^{-1}$.

ton sourced from a nucleus N , we have:

$$G_2^{el} = \left(\frac{a^2 t}{1 + a^2 t} \right)^2 \left(\frac{1}{1 + t/d} \right)^2 Z^2, \\ G_2^{in} = \left(\frac{a'^2 t}{1 + a'^2 t} \right)^2 \left(\frac{1 + \frac{t}{4m_p^2}(\mu_p^2 - 1)}{(1 + \frac{t}{0.71 \text{ GeV}^2})^4} \right) Z, \quad (20)$$

with the proton mass $m_p = 0.938$ GeV and $\mu_p = 2.79$.⁵ As noted in [72], an exchange of a very soft or very hard photon is suppressed due to either the screening from the electrons in the atomic cloud when

$$a^2 t, a'^2 t \ll 1, \quad a \equiv 111 \frac{1}{m_e Z^{1/3}}, \quad a' \equiv 773 \frac{1}{m_e Z^{2/3}} \quad (21)$$

or from the finite nuclear size in the other limit

$$t \gg d, \quad d = 0.164 \text{ GeV}^2 A^{-2/3}. \quad (22)$$

Although both the $g_{a\gamma}$ -driven Primakoff and g_{ae} -driven ALP bremsstrahlung processes share the same effective interaction with the target nuclei, it is interesting to point out that the former is strongly enhanced with respect to the latter. Indeed, in the regime $m_e \ll m_a \ll E_0$ one has the scaling:

$$\sigma_{ae} \propto \alpha_{\text{em}}^2 \frac{g_{ae}^2}{\pi} \frac{m_e^2}{m_a^2} \quad (23)$$

$$\sigma_{a\gamma} \propto \alpha_{\text{em}} g_{a\gamma}^2 \quad (24)$$

⁵Note that compared to the expression in [70] the last term of the inelastic form factor is not squared [71].

so that the bremsstrahlung process is suppressed with respect to Primakoff production due to its $2 \rightarrow 3$ kinematics and an extra α_{em} factor. In comparing with the case of a dark photon, it is worth noting that the typical equivalence holds:

$$e\varepsilon \leftrightarrow g_{ae}m_e , \quad (25)$$

up to order one factors from the different nature of the outgoing particles. This reflects a generic feature of our work: the electron ALP channel mimics the results for the dark photon (as could be broadly expected from the fact that the relevant production diagrams have a similar topology).

The final number of produced ALP in a given electron beam dump experiments is then given by:

$$\mathcal{N} = \frac{\mathcal{N}_A X_0 \rho}{A} \int_{E_c}^{E_0} dE \frac{\partial T_{e/\gamma}}{\partial E} \int_{E_c}^E dE_a \frac{d\sigma}{dE_a} \equiv \frac{\mathcal{N}_A X_0 \rho}{A} \sigma_{\text{eff}} \quad (26)$$

where we have include the possibility of an experimental energy cut-off E_c on the energy of the emitted ALP (with energy E_a), A is the atomic number of the dump medium, X_0 its track length (in cm) and ρ its mass density (in g cm^{-3}), the cross-section should then be expressed in cm^{-2} . We have defined in the last equality an “effective” cross-section, which includes the integration over the quantities $\frac{\partial T_{e/\gamma}}{\partial E}$. These differential track lengths represent the total length of material traversed by all e^\pm or γ of a given energy E present in the shower (expressed in unit of radiation length here). While the track lengths can be obtained directly via a simulation of the shower by a Monte-Carlo generator, a relatively reliable expressions for electron beam dump has been derived long ago in [73]:

$$\frac{\partial T_{e/\gamma}}{\partial E} = \int_0^{t_{\text{tar}}} dt I_{\gamma,e}(t, E) \quad \text{where} \quad \begin{cases} I_\gamma(t, E) = \frac{1}{E} \frac{(1 - E/E_0)^{4t/3} - e^{-7t/9}}{\frac{7}{9} + \frac{4}{3} \ln(1 - E/E_0)} \\ I_e(t, E) = \frac{1}{E} \frac{[\ln(E_0/E)]^{4t/3-1}}{\Gamma(4t/3)} \end{cases} , \quad (27)$$

where t_{tar} is the target length in unit of radiation length.

We have simulated both production processes in `MadGraph5_aMC@NLO` using an effective $NN\gamma$ interaction with form factor G_2 . This implies that we did not use the Weizsäcker-Williams approximation for the cross section, but instead estimated the $2 \rightarrow 3$ ($2 \rightarrow 2$ for the Primakoff case) processes. Furthermore, in order to regulate the numerical divergence which arises for large electron energies when the exchanged photon is very soft, we have modified the form factor $G_2(t)$. In particular, due to the screening effects occurring when $a^2 t \ll 1$, we know that this part of the phase space is sub-dominant in the final production rate. We therefore implemented a regularisation cut by setting the form factor to 0 in the “screened” region:

$$G_2^r(t) = \begin{cases} G_2(t) & \text{for } a^2 t > 1/3 \\ 0 & \text{for } a^2 t < 1/3 . \end{cases} \quad (28)$$

We have explicitly checked that the value of the final cross section is not modified by varying the cut between $a^2 t < 1$ and $a^2 t < 0.05$, and agrees with the analytical expression developed above. Furthermore, we have verified that the differential distribution in angles and energy are also not affected by this regularisation procedure.

We conclude this section by illustrating the hierarchy between both production modes in the case of the NA64 beam dump (described thoroughly in the next section) in Fig. 3. As expected, the photon-driven production strongly dominates the total rate, even though photons are strictly speaking secondary particles in the electromagnetic shower. This stems in part from the strong enhancement of the Primakoff production rate compared to the Bremsstrahlung one, and in part from the fact that bremsstrahlung photon carries in any case most of the energy of the scattered primary electron (with every primary electrons undergoing such a process as the NA64 target is around 40 radiation lengths).

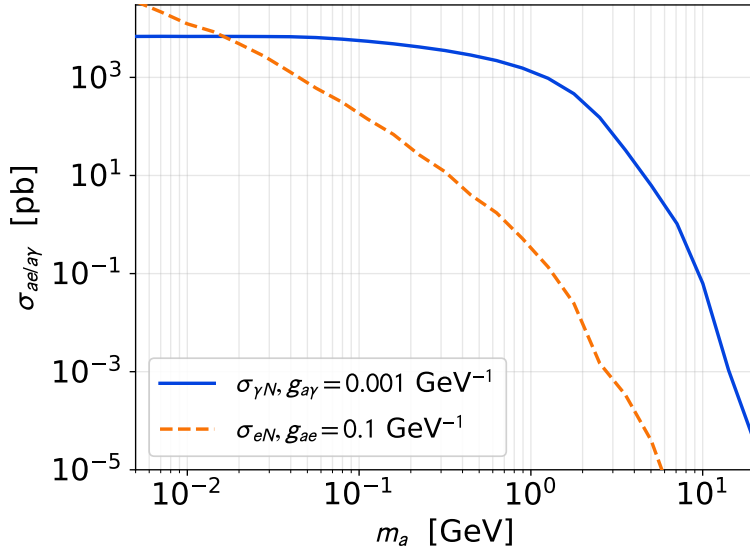


Figure 3: Effective production cross-section for the two dominant processes in NA64. The initial electron/photon energy is weighted by the track length distributions $\frac{\partial T_e}{\partial E} / \frac{\partial T_\gamma}{\partial E}$ for the corresponding particles in the electromagnetic shower.

3 Experimental searches for invisible ALPs

A trademark of the scenario presented above is that invisible channel dominates the ALP decay in all of the parameter range, in contrast with standard long-lived ALP searches. The signatures of such particle can be divided between “pure” missing energy searches, such as NA64, where one directly triggers on very low energy events created from high-energetic primaries; or “associated” missing energy searches, where the experiments use a single photon produced in association with the ALP to search for bumps on its recoil mass.

3.1 Limits from e^+e^- experiments

A first class of experiments rely on e^+e^- colliders to produce the ALP via the $e^+e^- \rightarrow a\gamma$ process and trigger on single photon events with a large missing energy from the escaping ALP. We will consider the re-interpretation of searches made in the BaBar [41] and DELPHI [40] experiments, as well as projections for Belle-II [43]. Due the ALP

decaying mainly invisibly, the LEP constraints [74] on $e^+e^- \rightarrow \gamma\gamma$ from visible mode are on the other hand not relevant here.

As was reviewed in the previous sections, the g_{ae} and $g_{a\gamma}$ couplings provide to a very good precision two independent production diagrams for the ALP, with suppressed interference effects. We can then define the total production rate times experimental efficiencies $(\epsilon\sigma)_{e^+e^-\rightarrow a\gamma}$ as the sum of the corresponding quantities for both production processes:

$$(\epsilon\sigma)_{e^+e^-\rightarrow a\gamma} = g_{ae}^2(\epsilon\sigma)_e + g_{a\gamma}^2(\epsilon\sigma)_\gamma , \quad (29)$$

where we have made the scaling in $g_{a\gamma}$ and g_{ae} explicit. Since all the experimental searches considered follow a “cut-and-count” strategies, this implies that we can estimate the limits g_{ae}^{lim} and $g_{a\gamma}^{\text{lim}}$ for both production process independently, then combine both rates to obtain the coupled limit $(g_{ae}, g_{a\gamma})_{\text{lim}}$

$$(g_{ae}, g_{a\gamma})_{\text{lim}} \leq \left(\left(\frac{g_{ae}^1}{g_{ae}^{\text{lim}}} \right)^2 + \left(\frac{g_{a\gamma}^1}{g_{a\gamma}^{\text{lim}}} \right)^2 \right)^{-1/2} \times (g_{ae}^1, g_{a\gamma}^1) , \quad (30)$$

where the input couplings $(g_{ae}^1, g_{a\gamma}^1)$ is only used to fix the ratio between both couplings. We will use the above approach for the DELPHI and PADME limits, for which we have fully simulated the expected signal. For BaBar and Belle-II projections, we will instead rely on comparing directly $(\epsilon\sigma)_{e^+e^-\rightarrow a\gamma}$ with the corresponding quantity for the dark photon model used in these experimental searches.

LEP-DELPHI The DELPHI experiment at LEP has performed a single-photon search [40] for invisibly decaying gravitons from low-scale extra-dimension which has been widely recasted for more generic invisible particles starting with [75].

We have simulated using `CalcHEP` [76] 10000 events with $e^+e^- \rightarrow \gamma + a$, and followed [75] and [40] in imposing the cuts

$$45^\circ < \theta_\gamma < 135^\circ \text{ and } 0.9 < E_\gamma/E_{\text{beam}} < 1.05 , \quad (31)$$

where θ_γ (E_γ) is the photon angle (energy) in the center-of-mass frame. Note that there is no correlation between E_γ and θ_γ , as is clear analytically since $E_\gamma = (s - m_a^2)/(4E_{\text{beam}})$. The DELPHI experiment quotes an energy resolution [40]:

$$\frac{\sigma_E}{E_\gamma} = 0.0435 \oplus \frac{0.32}{\sqrt{E_\gamma}} , \quad (32)$$

where \oplus denote the sum of two independent Gaussian distributions. This leads to a significant smearing of an otherwise narrow energy distribution centered around $E_\gamma = (s - m_a^2)/(4E_{\text{beam}})$, and is particularly important to model properly the threshold in m_a induced by the energy cuts $0.9 < E_\gamma/E_{\text{beam}} < 1.05$. Altogether, these cuts lead to a selection efficiency of around 40% for, e.g. $m_a = 10$ MeV and $g_{a\gamma} = 0.1$ GeV $^{-1}$.

It is important to point out that the CoM energy available at DELPHI varied during the full data taking, ranging between around 180.8 to 209.2 GeV [77]. We show the corresponding accumulated luminosity per energy bins in Table 1. Although this variation was not relevant in [75] which considered off-shell new physics operators whose effects were spread in the various energy bins, it is important to model properly

$\langle \sqrt{s} \rangle$ (GeV)	182.7	188.6	191.6	195.5	199.5	201.6	203.7	205.2	206.7	208.2
\mathcal{L} [pb $^{-1}$]	50.2	154.7	25.9	76.4	83.4	40.6	8.4	76.2	121.6	8.3

Table 1: Luminosity acquired in the DELPHI HPC detector as function of the average CoM energy delivered by LEP [77].

the above mass threshold. We have therefore estimated the efficiency for the energy cuts as a weighted sum over the luminosity per energy bins. Finally, we have included an overall $\varepsilon_t = 84\%$ trigger efficiencies following [75], leading to the full efficiency:

$$\varepsilon_{\text{DELPHI}} = \varepsilon_\theta \times \varepsilon_t \times \sum_i \frac{\mathcal{L}_i}{\mathcal{L}_{\text{tot}}} \varepsilon_{s_i} , \quad (33)$$

where ε_{s_i} is the efficiencies of the energy cuts for a LEP CoM energy $\sqrt{s_i}$ with luminosity \mathcal{L}_i given in Table 1, ε_θ is the efficiency of the angular cut (function of the ALP production process) and $\mathcal{L}_{\text{tot}} = 645.7 \text{ pb}^{-1}$ is the total luminosity. We illustrate this in Fig. 4, where we show the efficiencies of the angular and energy cuts, for the two main ALP production mechanisms. The dashed orange lines represents the efficiency in the case where all of the luminosity is assumed to be acquired at the average value $E_{\text{beam}} = 100$ GeV, while the full lines are the complete result. While both approaches are in good agreement for small ALP masses, they differ significantly around the threshold for ALPs mass close to the hundred of GeV. As can be further seen in Fig. 4, the associated production channel has an overall efficiencies much lower than the photon-induced s-channel process. This behaviour originate from the angular cuts and reflects the different shape of the angular differential distributions (with the associated production peaking at small angles).

For the statistical analysis of ALP production we need to compare the simulated signal events with the acquired data. One additional complication is that the predicted number of background events from the MC simulation in [40] agrees quite poorly with the actual data, particularly in the last bin. However, we note that the simulation $e^+e^- \rightarrow \gamma\nu\bar{\nu}$ performed a posteriori in [75] predicted around 49 such background events in the [0.9, 1.05], in better agreement with the 61 observed events. Altogether, a very conservative recasting of this analysis assuming that every observed events originated from an ALP signal leads to $N_{\text{lim}}^{90} \sim 72$ at 90%CL. A more aggressive limit includes instead the $e^+e^- \rightarrow \gamma\nu\bar{\nu}$ simulation from [75], assuming an overall 10% uncertainty on the background simulated in [75] (compared to the 5% systematics uncertainty cited in [77]), and assuming the rest to be produced by ALP production. This leads to $N_{\text{lim}}^{90} \sim 25.5$ at 90%CL, and an $\sim 40\%$ lower limit than the above choice. We will use the later choice when providing the final limits in the next sections, keeping in mind that this steams from somehow aggressive assumptions.

Once the limits g_{ae}^{lim} and $g_{a\gamma}^{\text{lim}}$ have been obtained for both ALP production processes as function of the ALP mass m_a , we can combine both limits as in Eq. (30).

BaBar The BaBar experiment at the PEP-II B-factory has accumulated a large dataset of e^+e^- collision events, corresponding to a total luminosity of 53 fb^{-1} . Single photon events with large missing energy were analysed via a bump-search [41], focusing on the case of a dark photon model. As such, the limits reported by the collaboration

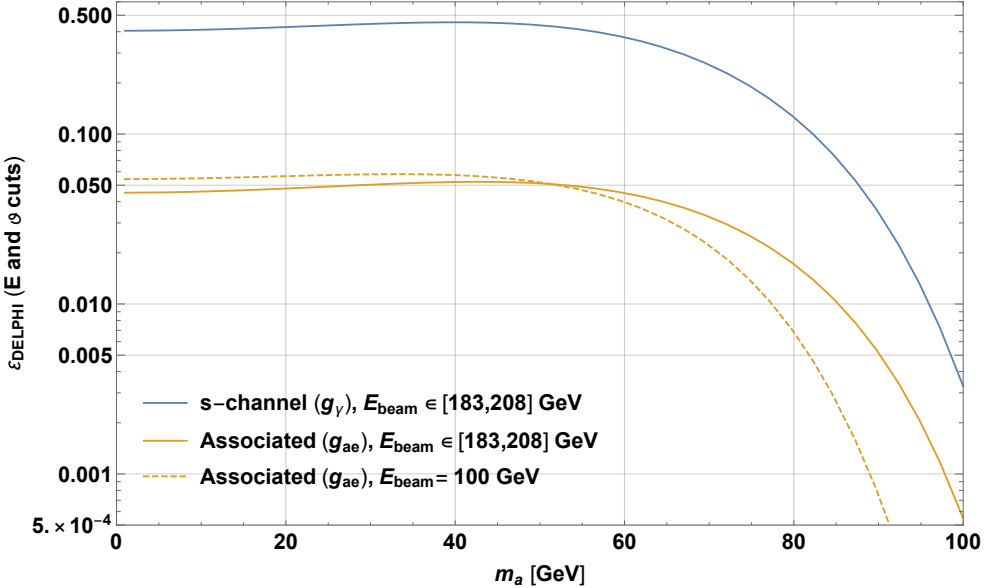


Figure 4: Total theoretical efficiencies for the energy cut $0.9 < E_\gamma/E_{beam} < 1.05$ and angular cut $45^\circ < \theta_\gamma < 135^\circ$ at DELPHI, both for the s-channel ALP production process and for the associated production one (depending respectively on $g_{a\gamma}$ and g_{ae}). We show in dashed line the efficiencies for associated production in the case of a fixed beam energy $E_{beam} = 100$ GeV.

need to be modified to account for the different production rates and kinematics of the ALP case.

We use the `CalcHEP` simulation setup introduced above tuned to the BaBar characteristics: an asymmetric interaction between 9 GeV electrons and 3.1 GeV positrons to produce a CoM collision energy of 10.58 GeV. The selection cut on the CoM angle

$$-0.4 < \cos \theta_\gamma < 0.6 \quad \text{for } m_a < 5.5 \text{ GeV} \quad (34)$$

$$-0.6 < \cos \theta_\gamma < 0.6 \quad \text{for } m_a > 5.5 \text{ GeV} , \quad (35)$$

were applied directly on the Monte-Carlo truth using Root [78]. Note that BaBar selection cuts further require $E_\gamma > 3$ (1.5) GeV for the low (high) mass search, but this cuts are redundant with the angular ones, up to around the threshold mass $m_a \sim 8$ GeV. We illustrate in Fig. 5 the energy and emission angle distributions for both the dark photon and the ALP case. As expected, both setups have a priori very distinct differential distributions. Note that since the photon energy is fixed in the CoM frame by $E_\gamma^{CoM} = (s - m_a^2)/(2\sqrt{s})$, the correlation between its laboratory frame energy and the angle θ is purely kinematic and does not depend on the nature of the emitted particle, being dark photon or ALP. On the other hand, as can be seen from Fig. 5, the efficiencies of the geometric cuts will vary strongly between both cases and thus need to be accounted for. Finally, we point out that the full BaBar analysis uses a Boosted-Decision-Tree (BDT) approach, whose efficiency as function of the signal characteristics (E_γ and θ_γ) is not reported. However, as is clear from Fig. 5, the actual distribution of signal events within the angular cuts are distinct (up to an overall normalisation factor) by at worse 25%. Hence the BDT variation in efficiency between both signal cannot be significantly larger than this number (since the BDT only consider the signal on an event-per-event basis), which we therefore consider as an uncertainty on our final result.

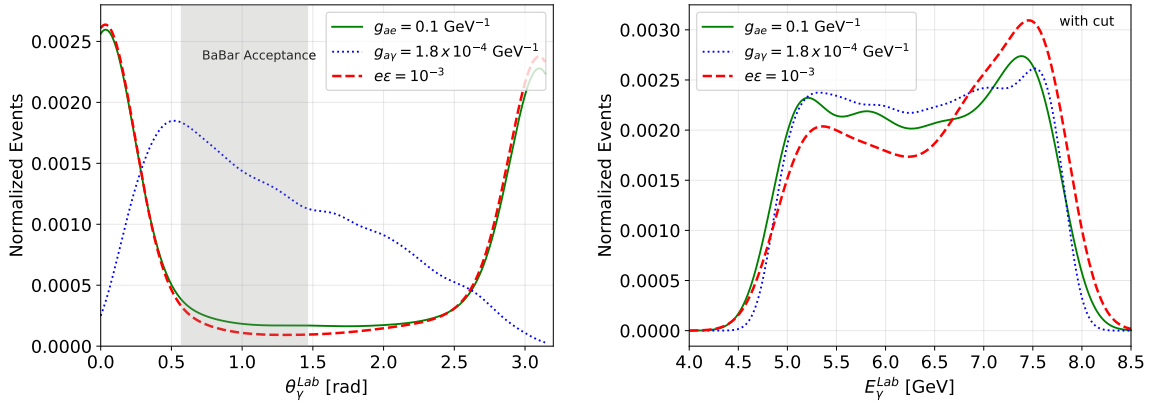


Figure 5: Normalized photon emission angle and energy (with Babar angular cut) distribution in the laboratory frame produced by $e^+e^- \rightarrow \gamma X$ process with $X =$ dark photon, ALP at $M_X = 20$ MeV. We assume $g_{a\gamma} = 1.8 \times 10^{-4}$ GeV $^{-1}$ (dotted blue) and $g_{ae} = 10^{-3}$ GeV $^{-1}$ (continuous green) for ALP model; $e\epsilon = 10^{-3}$ for dark photon model (dashed red). The grey region represents the BaBar angular coverage as described in the text.

In order to extend the limits from [41] to the case of an ALP with both $g_{a\gamma}$ and g_{ae} couplings, we have calculated the cross-section times efficiencies for $e^+e^- \rightarrow \gamma a$ in the acceptance of BaBar as function of the ALP mass. We then estimate its ratio with the one for a dark photon V of similar mass m_a and kinetic mixing $\epsilon = 10^{-3}$:

$$R(g_{a\gamma}, g_{ae}, m_a) \equiv \frac{(\epsilon\sigma)_e + (\epsilon\sigma)_a}{(\epsilon\sigma)_{e^+e^- \rightarrow \gamma V}} \quad (36)$$

The limit on the couplings is then given by:

$$(g_{ae}^{\lim}, g_{a\gamma}^{\lim}) = \left(\frac{\epsilon_{\text{BaBar}}^{\lim}}{0.001} \right) \frac{1}{\sqrt{R(m_a)}} \quad (37)$$

where $\epsilon_{\text{BaBar}}^{\lim}$ is the limit reported by the collaboration, and the final result only depends on the ratio between the ALP couplings $g_{ae}/g_{a\gamma}$ so that the ratio R can be for instance estimated on normalised couplings such that $g_{ae}^2 + g_{a\gamma}^2 = 1$ (or on any other choice leading to the same ratio $g_{ae}/g_{a\gamma}$).

Prospects for Belle-II The experiment Belle-II [43] is currently accumulating data and should present significantly stronger limits than BaBar in the coming years. Projection for mono-photon searches based on the same guiding principles as in BaBar have been given in [14, 43] based on a fast data acquisition of 20 fb^{-1} and a possible final experimental dataset of 50 ab^{-1} .

We have recasted the projection using the same approach as in the BaBar case. We estimated the expected number of events for both the dark photon and the ALP cases including the following experimental cuts (in the CoM frame):

$$-0.85 < \cos \theta_\gamma < 0.91 , \quad (38)$$

where we used the boost factor from laboratory to CoM frame at Belle-II of 0.28 (compared to 0.56 for BaBar) and the angular coverage of the triggers from [43]. Similarly

to the BaBar case we do not include directly the energy cuts since their effect is mostly included in the limits shown in [43]. Interestingly, due to the larger angular coverage, the kinematics differences between ALP-induced s-channel process and the dark photon one are somewhat larger than in the BaBar case (with dark photon distribution strongly localised around the upper limit of the mono-photon energy). This implies that a final accurate result for Belle-II limits on $g_{a\gamma}$ would require a dedicated simulation. Note that our actual recasting projection still agrees very well with the reach estimation performed in [14]. The same issue does not arise for the g_{ae} projections as the signal shares broadly the characteristics of the dark photon.

3.2 Limits from electron beam dump experiments

In a second time, let us focus on the limits arising from past and current electron beam dump experiments. Standard searches typically assume the ALP to decay visibly, and we thus expect limits from past electron beam dumps such as the one from the SLAC E141 [79] or SLAC E137 [44] experiments to be strongly suppressed. In the following we will illustrate this suppression by presenting the E137 limit as function of the ALP visible branching ratio. On the other hand, searches based at NA64 [42] do not always rely on a visible decay signal and will therefore lead to strong constraints.

E137 The SLAC E137 [44] experiment searched for light ALPs using a 20 GeV electron beam dumped into aluminium (later iron) plates interlaced with cooling water. The shielding was provided from a neighbouring hill, corresponding to $D = 179$ m of shielding, and was followed by $L = 204$ m of open air decay region. The electromagnetic calorimeter was $2\text{m} \times 3\text{m}$ ($3\text{m} \times 3\text{m}$) for Run 1 (Run 2) and could detect charged particles and/or photons. The experiment accumulated a total dataset of 1.86×10^{20} electrons on target (EoT), with one third during the first run (~ 10 C electrons) and the rest during Run 2 (~ 20 C electrons). No candidate events with an energy above ~ 2 GeV were found satisfying the various angular and timing cuts. Although one event was observed with energy higher than 1 GeV, there is a possibility it originates from a cosmic ray muon. [80]

In presence of both g_{ae} and $g_{a\gamma}$, the ALP will be predominantly produced by Primakoff effect, due to the suppression of the bremsstrahlung process as shown in Eq. (23).⁶ We will focus exclusively on this production mechanism in the following. Since this experiment assumed the visible decay of a long-lived ALP, it is clear that the reported limit should be significantly weakened in our setup. In order to estimate this effect, we will work from the recasting of [14], which used the experimental setup described above to deduce the upper limit from short-lived ALP based on the single, lower-limit given by the experimental collaboration [44].

In general, assuming that the detection and geometric efficiencies are solely a function of the ALP mass, the limits in the case of a significant invisible branching ratio for the ALP can be written from:

$$(g_{a\gamma}^{\text{new}})^2 = (g_{a\gamma}^{\text{old}})^2 \frac{\mathcal{P}^{\text{old}}}{\mathcal{P}^{\text{new}}} , \quad (39)$$

⁶Note that the presence of secondary positrons in the electromagnetic showers implies that resonant production of ALP can also occur, although with reduced geometric acceptance [81].

where we have used that the production rate of ALP is proportional to $g_{a\gamma}^2$, and defined \mathcal{P} the probability of a visible ALP decay in E137 decay volume as:

$$\mathcal{P}^{\text{new}} \equiv \exp\left(-\frac{(L+D)\Gamma_{\text{inv}}(g_{a\gamma}^{\text{new}})}{c\hbar\gamma_a}\right) \frac{L\Gamma_{\text{vis}}(g_{a\gamma}^{\text{new}})}{c\hbar\gamma_a} \quad (40)$$

$$\mathcal{P}^{\text{old}} \equiv \begin{cases} \exp\left(-\frac{D\Gamma_{\text{vis}}(g_{a\gamma}^{\text{old}})}{c\hbar\gamma_a}\right) & \text{for the upper, short-lived ALP limit} \\ \frac{L\Gamma_{\text{vis}}(g_{a\gamma}^{\text{old}})}{c\hbar\gamma_a} & \text{for the lower, long-lived ALP limit} \end{cases}, \quad (41)$$

where \mathcal{P}^{new} incorporates the probability that the ALP does not decay invisibly before the detector, and we have noted the ALP boost factor $\gamma_a = E_a/m_a$. The above formula further uses the fact that: (1) if the ALP decays mainly invisibly, the visible decay probability is small enough to approximate the exponential term by $\sim L\Gamma_{\text{vis}}(g_{a\gamma}^{\text{new}})$; (2) in the original case of visibly decaying ALP, the decay probability for the upper limit includes only the requirement that the ALP does not decay in the shielding. Indeed, since $L \gtrsim D$, the ALP will then decay in the decay volume with near 100% probability.

Altogether, it is clear that the only missing piece in this expression is the ALP boost factor, which depends on the ALP energy distribution after geometrical cuts applied. Interestingly, an average value as function of γ_a can be extracted from the above relations and the upper g_u and lower limits g_d given in [14] leading to:

$$\hbar c\langle\gamma_a\rangle = \frac{D\Gamma_{\gamma\gamma}(g_u)}{\mathcal{W}(g_u^4 D / (g_d^4 L))}, \quad (42)$$

where we have used the Lambert W function and $\Gamma_{\gamma\gamma}(g_u)$ is the ALP decay width to di-photon estimated for $g_{a\gamma} = g_u$. For small ALP masses, we found $m_a\langle\gamma_a\rangle \sim 15$ GeV, in accordance with the naive expectation given that E137 used a 20 GeV electron beam.⁷ Replacing in Eq. (39), we can then find the new upper limit in presence of a significant invisible ALP decay rate by solving for $g_{a\gamma}^{\text{new}}$ and using $g_{a\gamma}^{\text{old}} = g_d$ from [14].

Interestingly, the lower limit is not modified, as it corresponds to a regime where the ALP is long-lived, both for its visible and invisible decay. Consequently the number of expected visible decay events simply scales with the visible width, as in the standard case. The above relations could also be applied to other beam dump limits on visible ALP decay (see, e.g. [19] for a recent update).

An important comment is that while the ALP may decay invisibly, it is clearly possible that its decay products further leave a signal in the detector. A typical example of such mechanism could be light dark matter scattering, such as in the case of the dark photon (note however, that the higher dimensional nature of the ALP portal tends to suppress this contribution w.r.t the dark photon case). Another possibility is a three-body decay of some heavier dark sector states into a lighter one, as is typically found in inelastic dark matter scenarios. Since we do not specify the dark sector structure in this work, we will not include any such limits. Finally, it has been pointed out recently that inverse Primakoff process can also play a role [22].

⁷Note that in all beam dump experiments, the upper limits is typically dominated by the fraction of events with the highest boost factor since although one expect very large production rates, lower boost leads to an exponential suppression from early decay.

NA64 experiment Based on the CERN SPS, the NA64 experiment has access to a 100 GeV secondary electron beam. It has accumulated 2.84×10^{11} electron-on-target (EoT) during the 2016-2018 run, and is expected to reach overall 5×10^{12} EoT. The ALP production proceeds as in E137, with the Primakoff mechanism from secondary photon occurring directly within the electromagnetic calorimeter (ECAL), which can be modelled as 40 radiation lengths of lead.

Interestingly, the collaboration search [42] relies almost purely on a missing energy signatures, requiring that the total energy collected in the ECAL be smaller than 50 GeV (so that the ALP needs to carry at least 50 GeV away). No events were observed by the collaboration [42], in line with an expected background of around 0.19 ± 0.07 .

We have described in Sec. 2.3 a simple approximation to the ALP production rate in this scenario. Note that the requirement that the ALP carries at least half of the beam energy implies that only the onset of the electromagnetic shower in the ECAL will be relevant for this search. Including an experimental efficiency of around $\epsilon_{\text{NA64}} \simeq 50\%$, we find the expected number of events at NA64 as:

$$N_{\text{ALP}} = N_{\text{EoT}} \epsilon_{\text{NA64}} \times \mathcal{N}_A \frac{\rho_{Pb}}{A_{Pb}} X_{0,Pb} \times \left[\left(\frac{g_{ae}}{1 \text{ GeV}^{-1}} \right)^2 \sigma_{ae}^{\text{eff}} + \left(\frac{g_{a\gamma}}{1 \text{ GeV}^{-1}} \right)^2 \sigma_{a\gamma}^{\text{eff}} \right], \quad (43)$$

where N_{EoT} is the number of electrons on target, ρ_{Pb} is the lead mass density (11.4 g/cm^3), A_{Pb} is the lead atomic mass/atomic number and \mathcal{N}_A is the Avogadro number. We further used the effective cross-sections σ_{ae}^{eff} and $\sigma_{a\gamma}^{\text{eff}}$ which include the track-lengths integration as detailed in Eq. (26) and multiplied by the radiation length $X_{0,Pb} = 0.56$ cm to account for the normalisation of the track length distribution defined in Eq. (27). Note that the effective cross-sections account for the interaction between the beam and the nuclei in the target, so that they include factors of atomic number Z . We have estimated each effective cross-sections $\sigma_{a\gamma}^{\text{eff}}$ and σ_{ae}^{eff} using the numerical setup based on `MadGraph5_aMC@NLO` described in Sec. 2.3, using respectively $g_{a\gamma} = 1 \text{ GeV}^{-1}$ and $g_{ae} = 1 \text{ GeV}^{-1}$. We have included directly at the MC truth-level the energy cut, requiring the ALP to carry away 50 GeV. We put the 90%CL limit at 2.3 ALP events leading to current limits on g_{ae} and $g_{a\gamma}$ as well as prospects for the full NA64 dataset of 5×10^{12} EoT. Remarkably, our estimation of the limit agrees within 5% with the complete collaboration result in the low mass limit for m_a for the case of a pure photon-coupled ALP with $g_{ae} = 0$.⁸

3.3 Simulation of ALP production in the PADME environment

Based at LNF, the PADME experiment [45] uses a positron beam from the DAΦNE LINAC accelerator in fixed target configuration, using a polycrystalline diamond active target. The actual energy of the beam can be chosen and varied at will, up to around 550 MeV. The experiment is aiming to collect a sample of $N_{\text{poT}} \sim 4 \cdot 10^{13}$ positrons on target (poT) and has recently completed RUN II collecting already $\sim 5 \cdot 10^{12}$ poT. The current luminosity is mostly limited by the fact that the positron bunches are only 49 per second each containing ~ 28000 positrons, leading to significant pile-up in the experiment. Future experimental prospects include large improvements to the DAΦNE beam (POSEYDON proposal [47]) deserving the experiment, potentially spreading the

⁸The low mass limit corresponds to the case of the visibly decaying ALP searched for by the collaboration is long-lived, and hence mimics our signature.

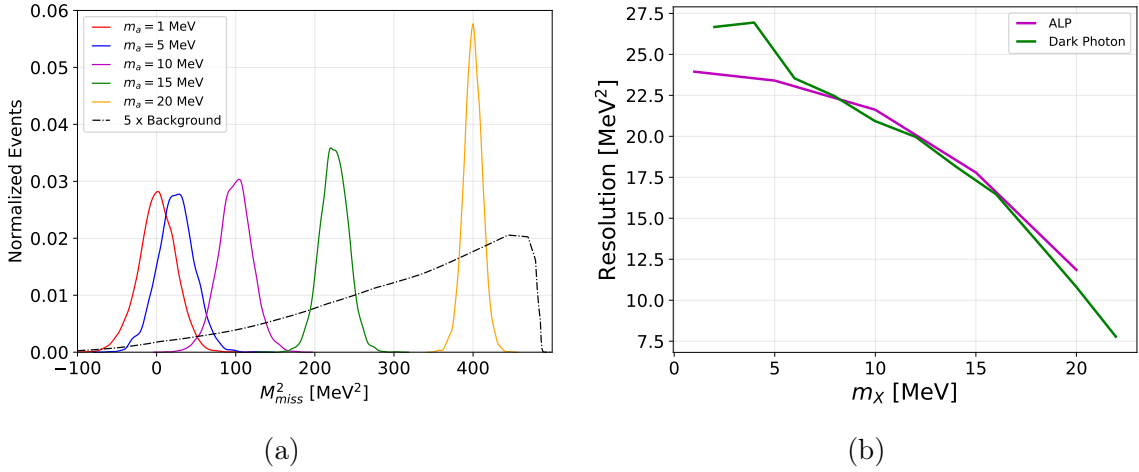


Figure 6: (6a) Normalized missing mass squared M_{miss}^2 distribution for some ALP masses with PADME cut applied, including energy and spatial resolution. The normalized distribution of background events (black dashed-dotted line) is extracted from [45]. (6b) Missing mass squared resolution as a function of dark particle mass m_X , ALP and dark photon. The energy of incident positron is $E_{beam} = 550$ MeV.

positron bunches and improving the possible N_{pot} to around $4 \cdot 10^{16}$ while reducing pile-up in the experiments (or even 10^{18} poT with similar pile-up).

The electromagnetic calorimeter (ECAL) is designed to measure the final photon 4-momentum. It is placed roughly 3.45m from the active target with a diameter of ~ 60 cm and consequently the following sets of basic cuts on the final-state are applied [82]:

- angular coverage: $(15 \lesssim \theta_\gamma \lesssim 80)$ mrad, with θ_γ the photon angle with respect to the beam in the laboratory frame;
- energy range for a reconstructed cluster in ECAL: $30 \text{ MeV} \lesssim E_\gamma \lesssim 500 \text{ MeV}$; ⁹

The adopted experimental technique of PADME relies on the measurement of the missing mass in the final state. Indeed knowing the initial conditions and measuring the photon four-momentum in the final state (P_γ) using the ECAL, it is possible to compute m_a^2 as the square of the missing mass M_{miss} :

$$M_{miss}^2 = (p_{e^+} + p_{e^-} - p_\gamma)^2.$$

Here p_i 's indicate the relativistic four-momentum of the corresponding particles. Therefore, the expected signal is represented by a peak at m_a^2 over a smooth distribution for the background $e^+e^- \rightarrow \gamma\gamma(\gamma)$ and Bremsstrahlung.

The Fig. (6a) shows the resulting squared missing mass distributions for some ALP masses along with a background estimate from [45] based on GEANT4 Monte Carlo simulation. The expected number of background events is around 3800 through the selection on 10^{11} simulated events. For reproducing the missing mass distribution we have simulated 10^5 events by **CalcHEP** and applied the PADME cut using Root. We

⁹Note that for the production of ALP+ γ , the photon emitted never reaches 500 MeV, even if the energy beam is equal to 550 MeV.

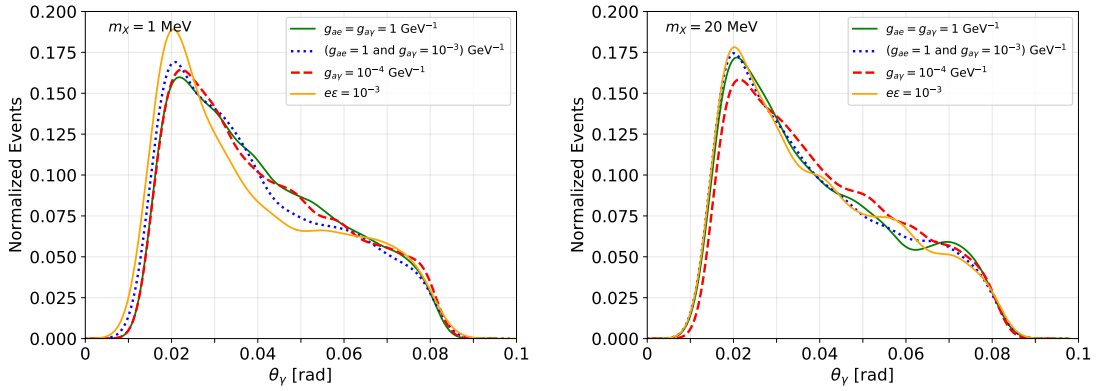


Figure 7: Normalized distribution of photon emission angle θ_γ produced by $e^+e^- \rightarrow \gamma X$ process with $X = \text{DP, ALP}$, at two different masses. We assume three set of couplings for our ALP model: $g_{a\gamma} = 1.8 \times 10^{-4} \text{ GeV}^{-1}$, $g_{ae} = 1 \text{ GeV}^{-1}$ and $g_{a\gamma} = 1 \text{ GeV}^{-1}$ or $g_{a\gamma} = 10^{-3} \text{ GeV}^{-1}$; the dark photon coupling is $ee = 10^{-3}$. The energy of incident positrons is $E_{beam} = 550 \text{ MeV}$.

have also included the spatial resolution of 4mm and the measured energy resolution of ECAL [82],

$$\frac{\sigma_E}{E_\gamma} = \frac{2\%}{\sqrt{E_\gamma[\text{GeV}]}} \oplus \frac{0.0003\%}{E_\gamma[\text{GeV}]} \oplus 1.1\%. \quad (44)$$

The missing mass resolution for ALP candidate in Fig. (6b) shows a good agreement with the technical design report of PADME for dark photon.

Including these selection cuts, the differential distribution of the final ALP events are, similarly to the case of BaBar, roughly equivalent to the one for a dark photon –up to an overall normalisation factor–. We illustrate this in Fig. 7, where we show the distribution of the photon emission angle w.r.t. to the beam θ_γ , for the case of a dark photon and of an ALP (both for s-channel and associated production processes). We have furthermore explicitly checked that the interference terms between the two ALPs production processes is negligible in all of our parameter range.

Altogether, we note that the higher ALP mass region is most affected by the cuts as the resonant behaviour of the associated (fermionic) channel, presenting a soft photon, is cut by the energy selection. This is illustrated in Fig. 8, where we show the ALP production cross-section after the cuts, as well the efficiency of the selection cuts for various ratios of $g_{ae}/g_{a\gamma}$. When the photon channel is larger than the fermion channel (black line), the selection cuts efficiencies is about 60% in all the ALP mass range until ~ 21 MeV. When the fermionic contribution is instead very large w.r.t. the photon one (orange line), the acceptance is much smaller, around 25% until $M_a \simeq 21$ MeV. In the region $m_a \gtrsim 21$ MeV, the energy cut reduces the signal down to zero as the energy of the photon emitted from electron and positron annihilation can only assume values smaller ~ 28 MeV. From these results, it is evident that both annihilation channels are important to search for $e^+e^- \rightarrow a\gamma$ signal. On the other hand, as the current limits on the $g_{a\gamma}$ limits are more stringent than on g_{ae} , PADME and its possible extension will be mostly relevant to probe the g_{ae} ALP interaction.

The expected number of events at PADME can then be obtained from the total

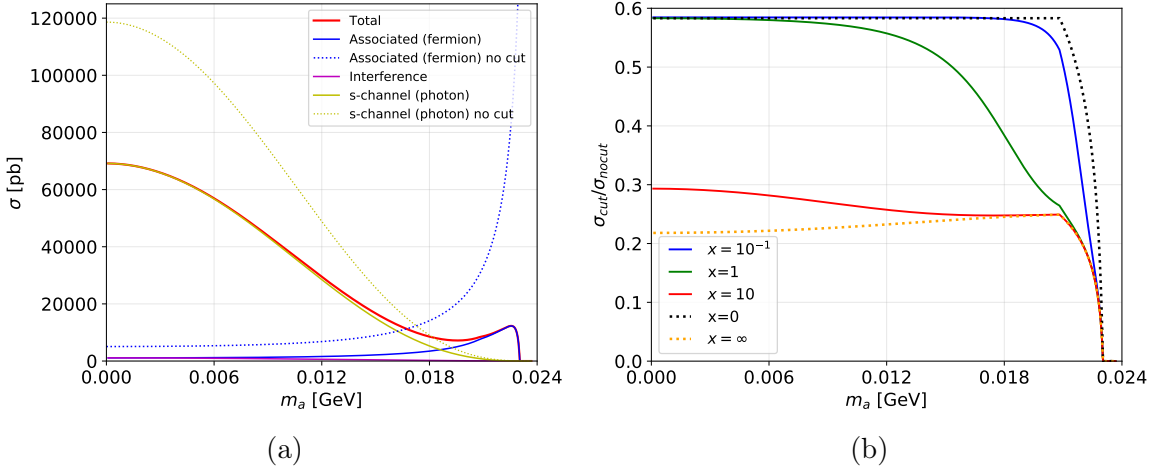


Figure 8: (a) Annihilation cross-section $e^+e^- \rightarrow \gamma+a$ as a function of ALP mass m_a for $g_{ae} = 1 \text{ GeV}^{-1}$ and $g_{a\gamma} = 1 \text{ GeV}^{-1}$ with PADME cut ($15 \lesssim \theta_\gamma \lesssim 80 \text{ mrad}$ and $30 \text{ MeV} \lesssim E_\gamma \lesssim 500 \text{ MeV}$). (b) Geometrical acceptance of the total cross-section imposing the $15 \lesssim \theta_\gamma \lesssim 80 \text{ mrad}$ and $30 \text{ MeV} \lesssim E_\gamma \lesssim 500 \text{ MeV}$ cuts as a function of ALP mass m_a for ratio of couplings $x = g_{ae}/g_{a\gamma}$. For both figures, the incident beam energy is $E_{beam} = 550 \text{ MeV}$.

production cross-section as

$$N_{ALP} = N_{poT} \mathcal{N}_A \frac{Z_C \rho_C}{A_C} d_t \times (\varepsilon_{PA} \sigma)_{\text{tot}} \quad (45)$$

where ρ_C/M_C is the carbon density (3.5 g/cm^3 for diamond), A_C is the carbon atomic mass (12 g/mol), $Z_C = 6$, the carbon atomic number and \mathcal{N}_A is the Avogadro number, $d_t = 100 \mu\text{m}$ is the thickness of the target and N_{poT} the number of positron on target. We have estimated the cross-section times efficiency $(\varepsilon \sigma_{\text{tot}})_{PA}$ using `CalcHEP`, including the selection cuts at PADME, for $g_{ae} = 1 \text{ GeV}^{-1}$ and $g_{a\gamma} = 1 \text{ GeV}^{-1}$ independently, denoted respectively $(\varepsilon_{PA} \sigma)_e$ and $(\varepsilon_{PA} \sigma)_\gamma$. We thus have:

$$(\varepsilon_{PA} \sigma)_{\text{tot}} = \left(\frac{g_{ae}}{1 \text{ GeV}^{-1}} \right)^2 (\varepsilon_{PA} \sigma)_e + \left(\frac{g_{a\gamma}}{1 \text{ GeV}^{-1}} \right)^2 (\varepsilon_{PA} \sigma)_\gamma \quad (46)$$

In order to estimate the background, we used the preliminary simulation as shown in [46]. The original aim of the collaboration was to perform a “bump hunt” search in M_{miss}^2 . As a conservative estimate, we have used the background events below the smeared resonance peak at 1.5σ (thus corresponding to 85% of the signal). In estimating the future experimental reach at POSEYDON, we assumed that detector improvements combined with reduced pile-up would lead to roughly the same number of background events despite the strongly increased dataset. We will thus show a 100-signal events line for the projection. Since the production rate depends on the couplings squares, the projected limit can be rescaled to the desired number of signal events n_s by multiplying it with $\sqrt{100/n_s}$. To illustrate the maximum possible reach we further show the single event sensitivity (SES), corresponding to 2.3 signal events. It is interesting to note that the possible successor to the PADME experiment running along the POSEYDON proposal $\sim 10^{16} \text{ poT/year}$ beam will inherit the technique but could have a different detector and hence different background rejection power. The actual limit will therefore depend on the performance of the new detector. In addition

the forward region $\theta < 15$ mrad and soft recoil photon, where most of the acceptance lies see Fig. 8a, could be explored by a 10^{16} poT experiment, reducing the pile up by factor of ~ 100 with respect to the current PADME setup.

Note that in case of the observation of a signal, the photon energy and emission angle (w.r.t. incident beam direction) correlation can give an information about the ALP mass. Fig. 9 shows how at small angles it is easier to distinguish the ALP mass while at small m_a the calorimeter resolution energy is crucial in order to distinguish them. The black dashed lines delimit the boundary of ECAL region.

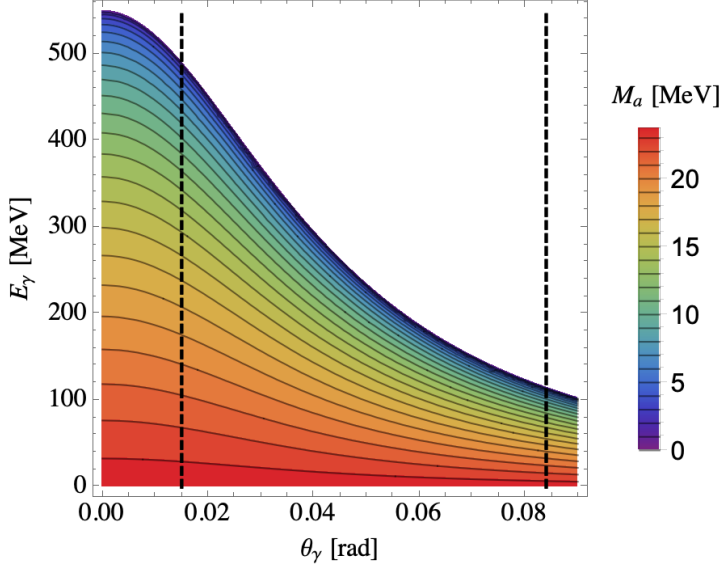


Figure 9: Correlation of the photon energy with its scattering angle. The gradient colour indicates the ALP mass. The dashed black lines are the angular separation between ECAL and SAC (Small Angle Calorimeter), and external ECAL border, respectively. The energy of the incident positron is $E_{beam} = 550$ MeV.

3.4 Magnetic moment of light leptons

The measured magnetic moment of the muon is one of the longest-standing anomaly of particle physics. Based on the original measurement at BNL [83] and on a string of improvements on the precision of the SM contribution (see e.g. the recent review [84]), the current discrepancy can be parametrised in terms of $a_\mu \equiv (g-2)_\mu/2$ as:

$$\Delta a_\mu \equiv a_\mu^{\text{SM}} - a_\mu = (2.79 \pm 0.76) \cdot 10^{-9} , \quad (47)$$

corresponding to a 3.7σ anomaly. Interestingly this measurement was recently complemented by a deviation in the corresponding quantity for the electron. Recent experimental improvements on the measurement of the fine structure constant based on the study of cesium-133 atoms in a matter-wave interferometers [85] coupled with the SM theoretical estimates [86] led:

$$\Delta a_e \equiv a_e^{\text{SM}} - a_e = -(8.7 \pm 3.6) \cdot 10^{-13} , \quad (48)$$

corresponding to a 2.4σ tension with the SM. Although the coincidence of these two anomalies is striking, their relative sign poses a significant theoretical challenge. Loop

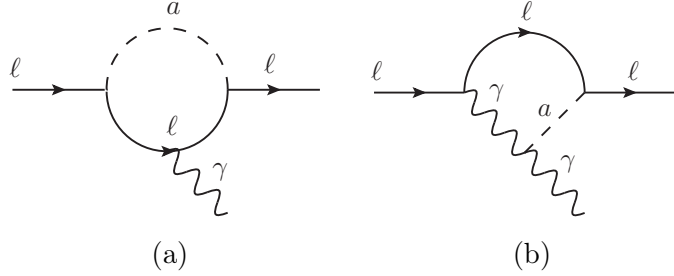


Figure 10: Feynman diagrams of the two main contributions to $\Delta a_e / \Delta a_\mu$ in our scenarios. We show in (a) the pure g_{ae} contributions and in (b) the mixed Barr-Zee diagram which scales as $g_{a\gamma} g_\ell$.

contributions from new light vector or scalar particles typically lead to a positive contribution to both Δa_e and Δa_μ , while contributions from axial vectors or pseudo-scalar are instead negative. Furthermore, as new physics contributions typically come proportional to squares of couplings, one generically expects a similar sign for both generation.

A light pseudo-scalar ALP provides one of the most elegant solution to explain both anomalies in one go, due to the simultaneous and generic presence of a photon and electron/muon couplings. We show the two main contributing diagrams in Fig. 10. Critically, the Barr-Zee type of diagrams are proportional to $g_{a\gamma} g_\ell$ and can therefore change sign depending on the sign of the fermion coupling involved [25, 87]. Summing further the pure fermionic contribution (see, e.g. [28]) as well as the 2-loop contribution from a light-by-light diagram [25] leads to the overall correction:

$$\Delta a_\ell = \frac{m_\ell^2}{16\pi^2} \left(2g_{a\gamma} g_{ae} (h_2 - \log \frac{\Lambda^2}{m_\ell^2}) - g_{ae}^2 h_1 + g_{a\gamma}^2 \frac{3\alpha_{\text{em}}}{\pi} \log^2 \frac{\Lambda}{m_\ell} \right), \quad (49)$$

where the loop function h_1 and h_2 are given as function of $x = \frac{m_a^2}{m_\ell^2}$ by:

$$h_1 = \int_0^1 \frac{2x^3}{x^2 + z(1-x)} \quad (50)$$

$$h_2 = 1 - \frac{x}{3} + \frac{x^2}{6} \log x + \frac{2+x}{3} \sqrt{x(4-x)} \arccos \frac{\sqrt{x}}{2}. \quad (51)$$

On the basis of the above expressions, the possibility of a simultaneous fit to both anomalies has been thoroughly explored in the literature since the Δa_e anomaly was pointed out. First attempts were based on a simplified model approach [26, 27], and then lepton-violating interactions were also used [28, 29]. In the following, we will focus on the flavour-diagonal case, which can typically explain both anomalies using only Barr-Zee diagrams, with a GeV-scale ALP for $g_{a\gamma} g_{ae} \sim 10^{-5} \text{ GeV}^{-2}$ and $g_{a\gamma} g_{ae} \sim -10^{-6} \text{ GeV}^{-2}$ (note the opposite sign).

Several comments are in order regarding the above mechanism. First, it is interesting to note that the contribution of g_{ae} to the electromagnetic anomaly, as discussed in Sec. 2, is precisely of the adequate order of magnitude to fit Δa_e with $g_{ae} \sim 0.01 - 0.1 \text{ GeV}^{-1}$. Additionally, while the required couplings to fermions are significant, we stress that this does not imply per-se that the corresponding scale Λ must be very small. From a UV perspective, the ALP interactions arise proportionally

to the charges of the broken approximate symmetry. A large coupling to, e.g. electrons, may thus simply indicate that they boast large charges. The above reasoning has been employed in various ways in the context of axion model building to boost selectively some axion couplings, see for instance [88]. We also note that such a UV-complete theory with non-universal ALP couplings to leptons will in general give rise to flavor-violating ALP-lepton interactions. We refer to [29, 89] for a thorough study of the constraints in this case. In the following, we will mostly focus on the case of the electron Δa_e anomaly, as we aim at constraining the ALP couplings to electrons and photons. We nonetheless will briefly comment on the muon anomaly by the end of this work. As a final comment, it is clear that the contributions from Eq. (49) do not include possible direct effects from the UV theory at the scale Λ . Given that both anomalies are known to be strongly sensitive to the presence of new particles up to the TeV scale, it is advisable to consider these anomalies more as potential guidelines to some type of new physics, rather than measurements that imply limits on equal footing with direct accelerator searches.

4 Results

Combining the results from the previous sections, we are now in position to provide an updated status for the search of (semi)-invisible ALPs. In the following plots, we will include when relevant the potential parameter ranges explaining the magnetic moment anomalies.

4.1 Photo-philic or electro-philic ALP

Let us first consider the standard case of a photo-philic ALP, in which we assume that the $g_{a\gamma}$ coupling dominates. We present in Fig. 11 the corresponding limits. It is clear that the mono-photon search from BaBar [41] dominates the constraints in most of the parameter range. In particular, and in contrast with the dark photon or visibly decaying ALP case, the missing energy search from NA64 [42] is sub-dominant in all of the parameter space. Nonetheless, we show that it could overcome the reach of BaBar with the full $5 \cdot 10^{12}$ EoT dataset, directly competing with the Belle-II reach for a primary dataset of 20 fb^{-1} . In the long run, the results from Belle-II will likely dominate the limits by an order of magnitude. In this parameter space, the PADME experiments does not lead to new parameter space covers and is not represented.

Interestingly, the limits from visible searches in beam dump experiments, such as E137 can remain relevant even with a largely suppressed ALP branching ratio into visible SM particles. We show this stability directly in Fig. 11: even with a visible branching ratio $\text{BR}_{\text{vis}}^{\text{ALP}} \equiv (\Gamma_{\gamma\gamma} + \Gamma_{e^+e^-})/\Gamma_{\text{inv}}$ as small as 10^{-4} (dot-dashed grey line), the E137 limit remain relevant in the lower mass part of the parameter space, mostly thanks to the saturation of BaBar and NA64 limits in this region. This implies that if one is interested into a partially invisible ALP, all beam dump limits need to be carefully estimated. Note that we do not represent the limit from Δa_e since given the strong current constraints on the photon coupling, the light-by-light contribution from Eq. (49) is typically negligible. Additionally, it has the wrong sign to explain the current measurement of Δa_e .

In a second time, we present instead the case of a purely electrophilic ALP. Due to the mass scaling of the electron bremsstrahlung cross-section showed in Eq. (23), the

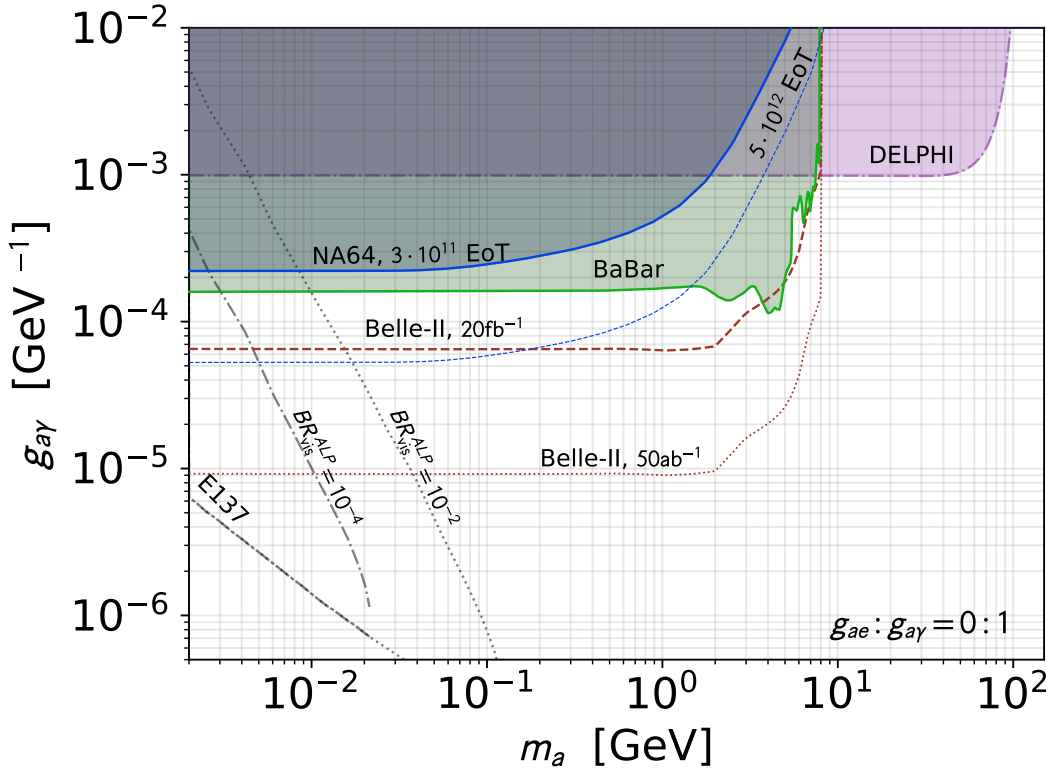


Figure 11: Summary of limits in the case where $g_{a\gamma}$ dominates over g_{ae} . Dashed grey lines indicate the exclusion range from E137 [44] for a 10^{-2} and 10^{-4} branching ratio. The purple region is the exclusion from DELPHI mono-photon [40, 75]. In blue are shown the current and future limits from NA64 [42]. The green region is the exclusion from mono-photon search at BaBar [41], and dashed rust lines the prospects at Belle-II [43] for a 20 fb^{-1} and 50 ab^{-1} dataset.

limits from electron beam dump, and in particular at NA64, increases in the low mass regime. Altogether, and in line with the general scaling argument presented in Sec. 2, the limits follow the same hierarchy as the better known case of a dark photon portal. NA64 dominates in the lower mass ranges (below around 200 MeV), while BaBar and soon-to-be release results from Belle-II provide the strongest constraints up to around 10 GeV. Probing the higher mass range is significantly harder in intensity frontier experiments, so that LEP mono-photon searches still provide the strongest bounds in the tens of GeV range. It is worth noting that in this region the “pure” g_{ae} contribution to Δa_e could still lead to an explanation of the experimental measurement, although most of the relevant parameter space is already excluded. In a five-year time-scale, we additionally note that improvement of the PADME experimental setup could probe a part of the same parameter space as the NA64 experiment with its full expected dataset.

4.2 Combined case

Let us now turn to the case where both couplings are present in the theory. We show the corresponding limits in Fig. 13 for an ALP mass $m_a = 0.01, 1$ and 7.5 GeV . In most cases the presence of both couplings do not lead to a striking new behaviour. Instead,

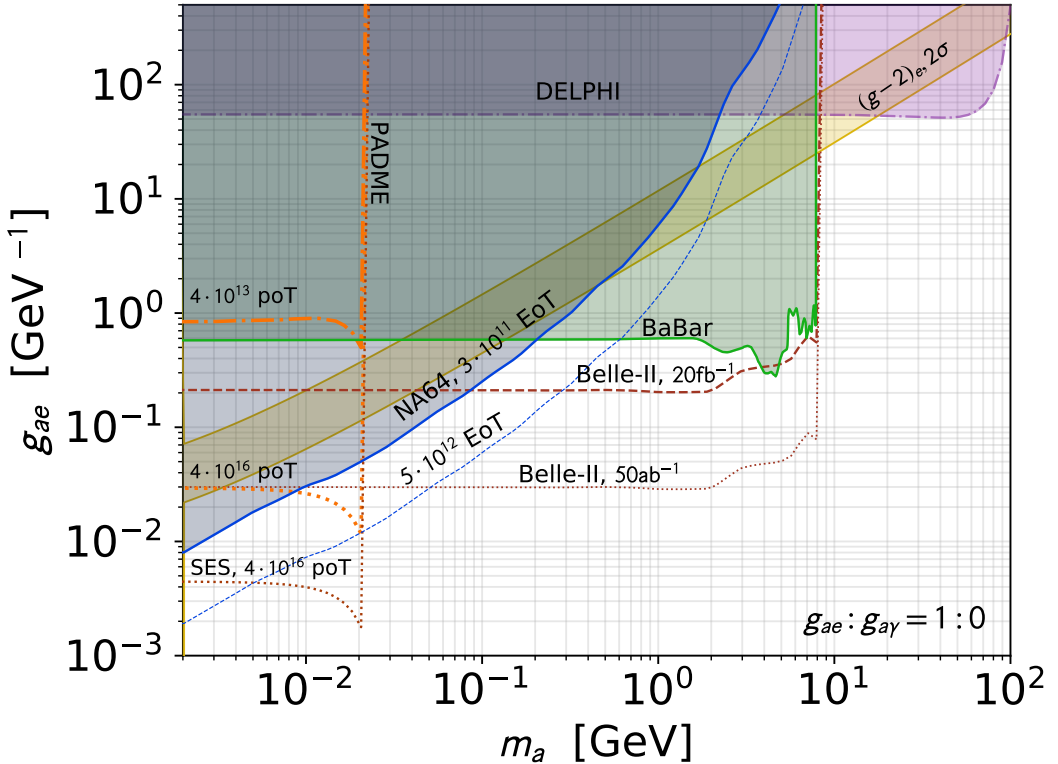


Figure 12: Summary of limits in the case where g_{ae} dominates over $g_{a\gamma}$. The dashed orange lines are (top to bottom) the projection for PADME [46] for the current run, and for a POSEYDON [47] extension with either 100 signal events, or with single-event sensitivity (SES - 2.3 events line). The purple region is the exclusion from DELPHI mono-photon [40, 75]. In blue are shown the current and future limits from NA64 [42]. The green region is the exclusion from mono-photon search at BaBar [41], and dashed rust lines the prospects at Belle-II [43] for a 20 fb^{-1} and 50 ab^{-1} dataset. The gold region corresponds to the 2σ range for the $(g-2)_e$ anomaly.

a smooth transition is observed when both electron and photon contribution to the production rate are similar. The first important exception is the residual limit which can be obtained for beam dump experiments, illustrated by the E137 bounds shown as the grey area (for the case where the ALP visible branching ratio is 10^{-4}). Indeed, both photons or electrons can mediate the ALP decays. This implies that although we have only included ALP production via the Primakoff mechanism, the electron channel is the main visible ALP decay channel in the right-hand part of Fig. 13. Our assumption that ALP invisible decay dominates then implies that the limit at $m_a = 10$ MeV stops around $g_{ae} \sim 10^{-4}$ where the ALP invisible decay length becomes much smaller than the length of the shielding. The second observable which depends non-trivially on both couplings is the magnetic moment Δa_e . The combination of both the pure g_{ae}^2 contribution with the mixed Barr-Zee $g_{ae}g_{a\gamma}$ term leads to the opening of relevant parameter space in the low mass region below the current NA64 and BaBar limits. The experimental prospects in this region is also very good, as this anomaly provides a clear target for future improvements in NA64, PADME and in Belle-II. The 2σ range (shown as the gold region in the figures) is therefore likely to be covered almost entirely in the near future, in particular thanks to future Belle-II limits. Finally, the

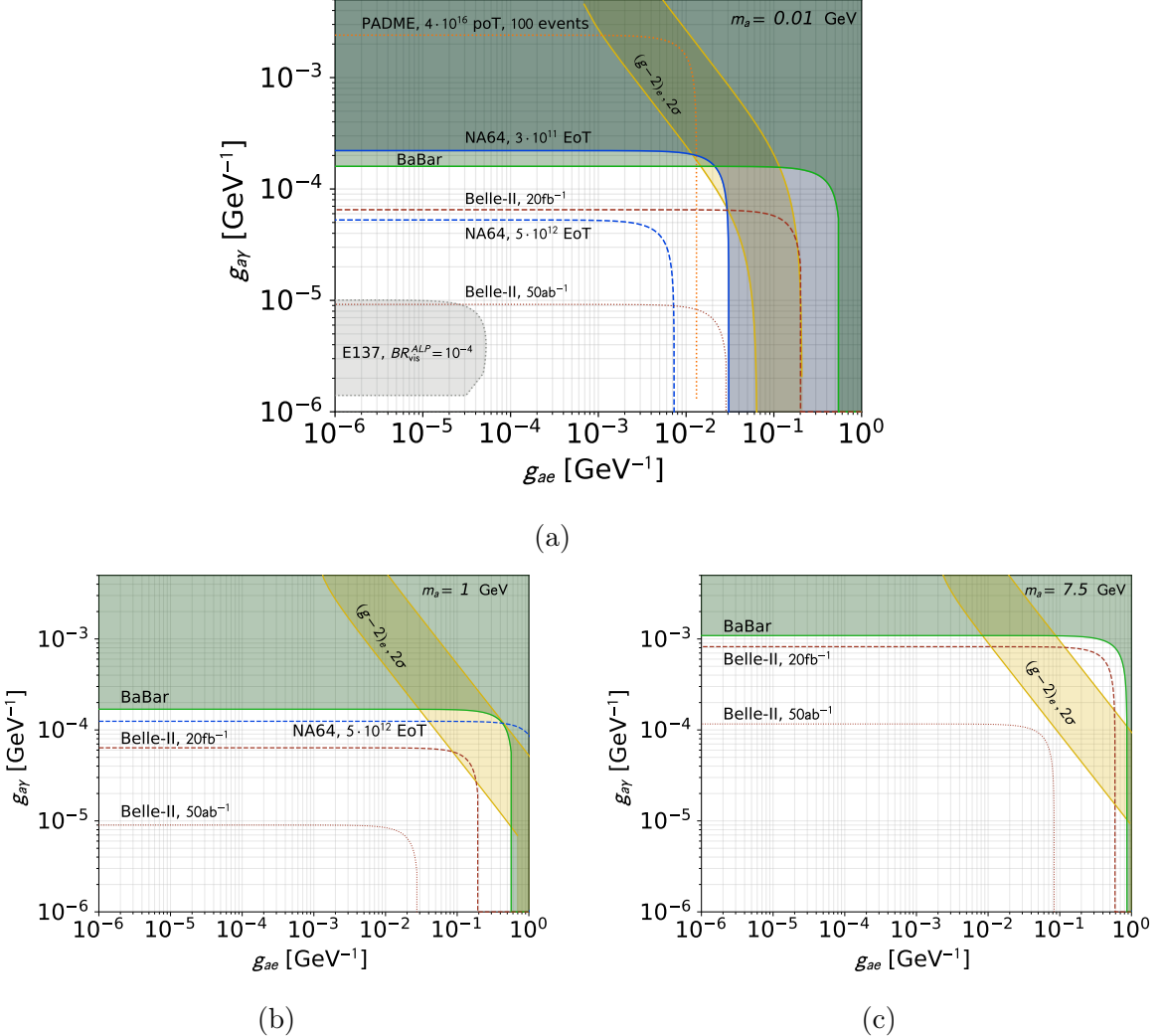


Figure 13: Summary of limits as function of g_{ae} and $g_{a\gamma}$ for $m_a = 10$ MeV (13a), $m_a = 1$ GeV (13b) and $m_a = 7.5$ GeV (13c). The dashed grey line and grey area indicate the exclusion range from E137 [44] for a 10^{-4} visible branching ratio. The dashed orange lines are (top to bottom) the projection for PADME [46] for the current run, and for a POSEYDON [47] extension with either 100 signal events, or with single-event sensitivity (SES - 2.3 events line). The purple region is the exclusion from DELPHI mono-photon [40,75]. In blue are shown the current and future limits from NA64 [42]. The green region is the exclusion from mono-photon search at BaBar [41], and dashed rust lines the prospects at Belle-II [43] for a 20 fb^{-1} and 50 ab^{-1} dataset. The gold region corresponds to the 2σ range for the $(g - 2)_e$ anomaly.

relationship between the limits from NA64 and BaBar is of interest. While the former is typically relevant only at low ALP mass, is dominates the constraints in g_{ae} but not in $g_{a\gamma}$. This can be traced back in a large part to the $1/s$ suppression of the associated cross-section in electron-positron collider.

We investigate further the mass dependence of these limits in Fig. 14. We show the limits on the ALP couplings as function of its mass for both $g_{a\gamma}/g_{ae} = 0.01$ and $g_{a\gamma}/g_{ae} = 0.001$. The latter choice corresponds roughly to the expected size of radiatively-generated photon-ALP couplings. In both cases, the limits are typically dominated by the photon-induced processes, particularly for BaBar and Belle-II, while NA64 transitions between both regimes as function of the ALP mass (with g_{ae} -driven

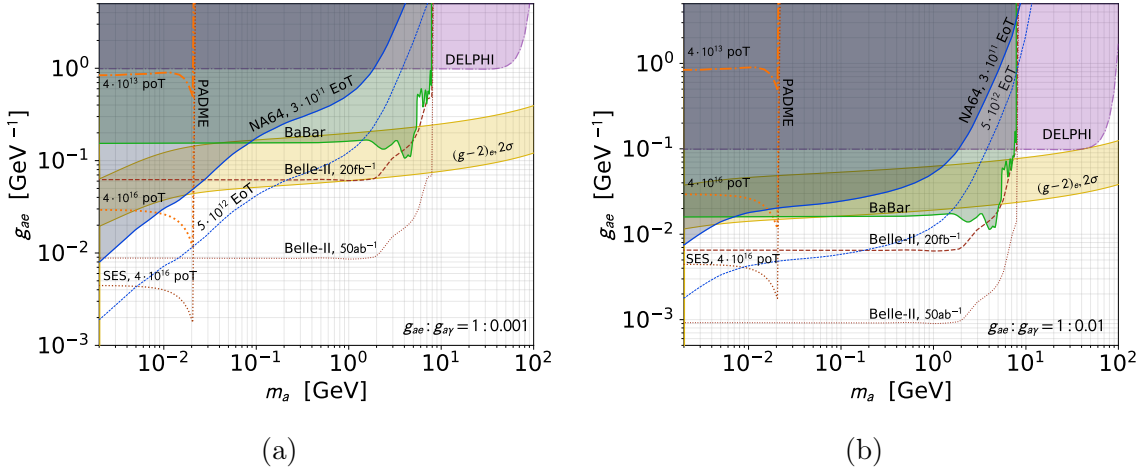


Figure 14: Summary of limits as function of g_{ae} and m_a for $g_{ae}/g_{a\gamma} = 0.001$ (14a) and $g_{ae}/g_{a\gamma} = 0.01$ (14b). A negligible ALP visible branching ratio is assumed. The dashed orange lines are (top to bottom) the projection for PADME [46] for the current run, and for a POSEYDON [47] extension with either 100 signal events, or with single-event sensitivity (SES - 2.3 events line). The purple region is the exclusion from DELPHI mono-photon [40, 75]. In blue are shown the current and future limits from NA64 [42]. The green region is the exclusion from BaBar [41], and dashed rust lines the prospects at Belle-II [43] for a 20 fb^{-1} and 50 ab^{-1} dataset. The gold region corresponds to the 2σ range for the $(g-2)_e$ anomaly.

constraints dominating at low mass). The figure also illustrate the large parameter space still available for an electrophilic-ALP solution to the Δa_e anomaly, with parameter space extending down to tens of MeV. In absence of any significant UV contribution, one can see the area above the gold region as excluded by the Δa_e measurement. However, the ALP formalism is by definition a low energy effective theory precisely relying on the presence of a larger UV field content. One should therefore be cautious about assuming that there will be no other meaningful contributions to Δa_e .

We conclude this section by extending slightly our model by including an additional muonic interaction $g_{a\mu}$ in order to fit simultaneously both the Δa_e and Δa_μ anomalies. We show in Fig. 15 the preferred range when fixing the ratio $g_{ae} \sim -10g_{a\mu}$. As expected from previous results (see e.g. [29]) the choice $g_{ae} \sim -10g_{a\mu}$ provides a very good fit in a large mass range. It is however notable that the combined region extends to much lower mass than what was investigated previously, as the final results from BaBar are in fact not sufficient to exclude the Δa_μ -favoured region below 10 GeV. Moreover, it is interesting to remark that the radiative prediction for the ratio $g_{a\gamma}/g_{ae} \sim 0.001$ leads to an adequate range for the photon interaction. Indeed this ratio offers a good compromise between a suppression of the accelerator limits (and in particular of BaBar) and a large enough enhancements of both Δa_e and Δa_μ via the Barr-Zee diagram contribution. Note that we did not included projected limits on the ALP muon couplings from past (e.g. E137 limits [90]) and possible future experiments such as for instance NA64- μ [91], M^3 [92] or dedicated Belle-II searches [93]. Given that we expect the ALP muon coupling to be smaller than the electron one, the latter should dominate the limits in the near future.

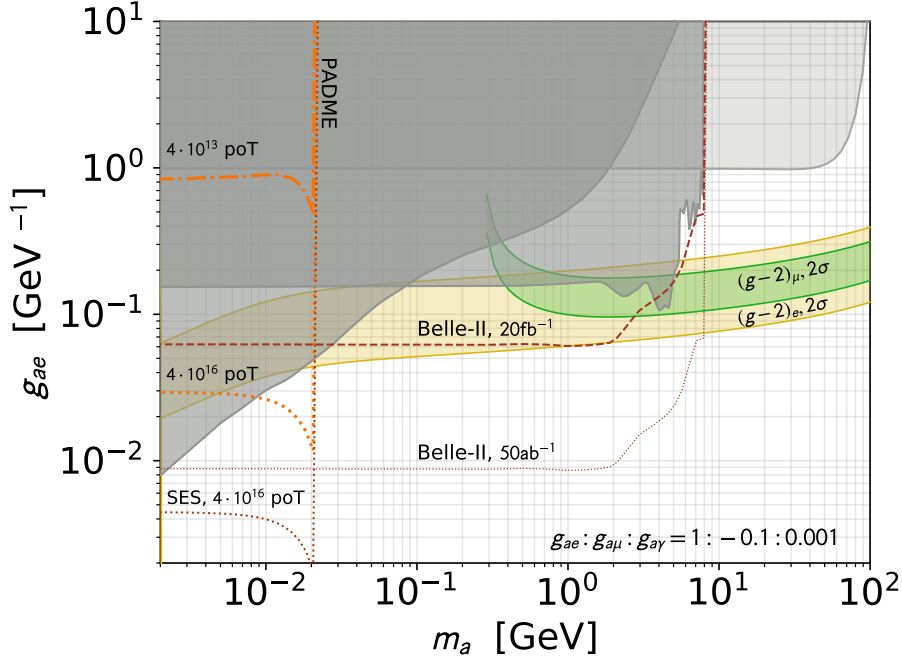


Figure 15: The invisible ALP $(g-2)_{e,\mu}$ solution. Summary of limits for $g_{ae}/g_{a\gamma} = 0.001$ and $g_{a\mu}/g_{a\gamma} = -0.01$. The dashed orange lines are (top to bottom) the projection for PADME [46] for the current run, and for a POSEYDON [47] extension with either 100 signal events, or with single-event sensitivity (SES - 2.3 events line). The grey regions covers the exclusion from DELPHI [40, 75], NA64 [42] and BaBar [41]. The dashed rust lines are the prospects at Belle-II [43] for a 20 fb^{-1} and 50 ab^{-1} dataset. The gold region corresponds to the 2σ range for the $(g-2)_e$ anomaly and the green region to the 2σ range for the $(g-2)_\mu$ anomaly.

5 Conclusions

We have presented in this work a thorough analysis of the existing limits lying on models of ALP-portals, in which an ALP coupling mainly with electrons and photons in the visible sector, is further assumed to decay invisibly into additional dark sector states. Reviewing first some of the standard astrophysical aspects of such a setup, we have shown in particular that interactions within the dark sector may be enough to escape successfully limits from the duration of the SN1987 neutrino burst. Indeed, focusing in the case of a single dark fermion as an example, we have shown that reasonable dark sector interactions may maintain this fermion in equilibrium with the ALP population in the pseudo-neutron star core, thus placing the parameter space accessible to earth-based experiments in the usual ‘‘trapping regime’’.

We have then performed a thorough re-interpretation of all the relevant collider and beam dump experiments relevant to our setup, something which had not been done for the case of an invisible ALP with electron couplings. As the ALP is expected to decay invisibly, the dominant constraints arose from in the various missing energy searches in BaBar, NA64 and mono-photon searches at LEP. We based our LEP limit on a DELPHI mono-photon search already widely used to constraint both an invisible dark photon and an invisible ALP, but include for the first time the variation of the LEP center-of-mass energy during the run time. This has the main effect of shifting the mass threshold of this analysis to larger ALP masses. We additionally re-interpret NA64 limits on a

visible ALP to a purely invisible search, mimicking to a certain extend the results found by the collaboration for the case of an invisible dark photon. Interestingly, we have also shown that completely relaxing the limits from existing searches for long-lived ALP decays is challenging and requires a significant suppression of the visible ALP branching ratios. We illustrate this point in the case of the E137 beam dump experiment, although the formalism presented above could allow in principle to recast other beam-dump based long-lived ALP search. Finally we have investigate a future reach for the PADME positron beam dump experiment current run, and shown tentative projections for the future experimental improvements of the DAΦNE beam line following the POSEYDON proposal.

The invisible ALP investigated in this work represents one of the prime new physics candidate to explain the recently found anomaly in the magnetic moment of the electron. We have combined the limits found above with the current ALP parameter range hinted at by the anomaly, finding that it provides an extremely attractive experimental targets for upcoming experiments. In particular, we expect both the NA64 and the Belle-II collaboration to probe in a large extent the relevant region for ALP mass below 10 GeV in the very near future. The Belle-II experiments could especially test with only 20 fb^{-1} most of the parameter space up to the 10 GeV mass threshold. The combined ALP solution for both Δa_e and Δa_μ anomalies has been additionally found to be viable down to hundred of MeV, thanks to the significant weakening of the existing BaBar limits in the electron channel, further providing a golden target for future experimental probes.

Acknowledgments

We acknowledge discussions with L. Delle Rose and R. Simeonov at the beginning of the project, and P. Valente for providing us with the details of the DAΦNE POSEYON setup. L.D. thanks F. Kahlhoefer for useful feedback on ALP astrophysics. L.D. and E.N. acknowledge the PADME collaboration for fundamental inputs on the experimental analysis. L.D. and E.N. are supported in part by the INFN “Iniziativa Specifica” Theoretical Astroparticle Physics (TAsP-LNF).

References

- [1] F. Wilczek, “Axions and Family Symmetry Breaking,” *Phys. Rev. Lett.* **49** (1982) 1549–1552.
- [2] Y. Chikashige, R. N. Mohapatra, and R. Peccei, “Are There Real Goldstone Bosons Associated with Broken Lepton Number?,” *Phys. Lett. B* **98** (1981) 265–268.
- [3] G. Gelmini and M. Roncadelli, “Left-Handed Neutrino Mass Scale and Spontaneously Broken Lepton Number,” *Phys. Lett. B* **99** (1981) 411–415.
- [4] R. D. Peccei and H. R. Quinn, “CP Conservation in the Presence of Instantons,” *Phys. Rev. Lett.* **38** (1977) 1440–1443.
- [5] R. D. Peccei and H. R. Quinn, “Constraints Imposed by CP Conservation in the Presence of Instantons,” *Phys. Rev. D* **16** (1977) 1791–1797.
- [6] S. Weinberg, “A New Light Boson?,” *Phys. Rev. Lett.* **40** (1978) 223–226.
- [7] F. Wilczek, “Problem of Strong P and T Invariance in the Presence of Instantons,” *Phys. Rev. Lett.* **40** (1978) 279–282.
- [8] A. Arvanitaki, S. Dimopoulos, S. Dubovsky, N. Kaloper, and J. March-Russell, “String Axiverse,” *Phys. Rev. D* **81** (2010) 123530, [arXiv:0905.4720 \[hep-th\]](https://arxiv.org/abs/0905.4720).
- [9] M. Cicoli, M. Goodsell, and A. Ringwald, “The type IIB string axiverse and its low-energy phenomenology,” *JHEP* **10** (2012) 146, [arXiv:1206.0819 \[hep-th\]](https://arxiv.org/abs/1206.0819).
- [10] A. Hook, “Anomalous solutions to the strong CP problem,” *Phys. Rev. Lett.* **114** no. 14, (2015) 141801, [arXiv:1411.3325 \[hep-ph\]](https://arxiv.org/abs/1411.3325).
- [11] H. Fukuda, K. Harigaya, M. Ibe, and T. T. Yanagida, “Model of visible QCD axion,” *Phys. Rev. D* **92** no. 1, (2015) 015021, [arXiv:1504.06084 \[hep-ph\]](https://arxiv.org/abs/1504.06084).
- [12] P. W. Graham, D. E. Kaplan, and S. Rajendran, “Cosmological Relaxation of the Electroweak Scale,” *Phys. Rev. Lett.* **115** no. 22, (2015) 221801, [arXiv:1504.07551 \[hep-ph\]](https://arxiv.org/abs/1504.07551).
- [13] M. Bauer, M. Neubert, and A. Thamm, “Collider Probes of Axion-Like Particles,” *JHEP* **12** (2017) 044, [arXiv:1708.00443 \[hep-ph\]](https://arxiv.org/abs/1708.00443).
- [14] M. J. Dolan, T. Ferber, C. Hearty, F. Kahlhoefer, and K. Schmidt-Hoberg, “Revised constraints and Belle II sensitivity for visible and invisible axion-like particles,” *JHEP* **12** (2017) 094, [arXiv:1709.00009 \[hep-ph\]](https://arxiv.org/abs/1709.00009).
- [15] M. Bauer, M. Heiles, M. Neubert, and A. Thamm, “Axion-Like Particles at Future Colliders,” *Eur. Phys. J. C* **79** no. 1, (2019) 74, [arXiv:1808.10323 \[hep-ph\]](https://arxiv.org/abs/1808.10323).
- [16] J. L. Feng, I. Galon, F. Kling, and S. Trojanowski, “Axionlike particles at FASER: The LHC as a photon beam dump,” *Phys. Rev. D* **98** no. 5, (2018) 055021, [arXiv:1806.02348 \[hep-ph\]](https://arxiv.org/abs/1806.02348).

- [17] L. Harland-Lang, J. Jaeckel, and M. Spannowsky, “A fresh look at ALP searches in fixed target experiments,” *Phys. Lett. B* **793** (2019) 281–289, [arXiv:1902.04878 \[hep-ph\]](https://arxiv.org/abs/1902.04878).
- [18] D. Aloni, C. Fanelli, Y. Soreq, and M. Williams, “Photoproduction of Axionlike Particles,” *Phys. Rev. Lett.* **123** no. 7, (2019) 071801, [arXiv:1903.03586 \[hep-ph\]](https://arxiv.org/abs/1903.03586).
- [19] B. Döbrich, J. Jaeckel, and T. Spadaro, “Light in the beam dump - ALP production from decay photons in proton beam-dumps,” *JHEP* **05** (2019) 213, [arXiv:1904.02091 \[hep-ph\]](https://arxiv.org/abs/1904.02091). [Erratum: JHEP 10, 046 (2020)].
- [20] F. Ertas and F. Kahlhoefer, “On the interplay between astrophysical and laboratory probes of MeV-scale axion-like particles,” *JHEP* **07** (2020) 050, [arXiv:2004.01193 \[hep-ph\]](https://arxiv.org/abs/2004.01193).
- [21] Y. Sakaki and D. Ueda, “Search for new light particles at ILC main beam dump,” [arXiv:2009.13790 \[hep-ph\]](https://arxiv.org/abs/2009.13790).
- [22] V. Brdar, B. Dutta, W. Jang, D. Kim, I. M. Shoemaker, Z. Tabrizi, A. Thompson, and J. Yu, “Axion-like Particles at Future Neutrino Experiments: Closing the ”Cosmological Triangle”,” [arXiv:2011.07054 \[hep-ph\]](https://arxiv.org/abs/2011.07054).
- [23] D. Kirpichnikov, V. E. Lyubovitskij, and A. S. Zhevlakov, “Implication of hidden sub-GeV bosons for the $(g - 2)_\mu$, ${}^8\text{Be} - {}^4\text{He}$ anomaly, proton charge radius, EDM of fermions, and dark axion portal,” *Phys. Rev. D* **102** no. 9, (2020) 095024, [arXiv:2002.07496 \[hep-ph\]](https://arxiv.org/abs/2002.07496).
- [24] D. Chang, W.-F. Chang, C.-H. Chou, and W.-Y. Keung, “Large two loop contributions to $g-2$ from a generic pseudoscalar boson,” *Phys. Rev. D* **63** (2001) 091301, [arXiv:hep-ph/0009292](https://arxiv.org/abs/hep-ph/0009292).
- [25] W. Marciano, A. Masiero, P. Paradisi, and M. Passera, “Contributions of axionlike particles to lepton dipole moments,” *Phys. Rev. D* **94** no. 11, (2016) 115033, [arXiv:1607.01022 \[hep-ph\]](https://arxiv.org/abs/1607.01022).
- [26] J. Liu, C. E. Wagner, and X.-P. Wang, “A light complex scalar for the electron and muon anomalous magnetic moments,” *JHEP* **03** (2019) 008, [arXiv:1810.11028 \[hep-ph\]](https://arxiv.org/abs/1810.11028).
- [27] F. Abu-Ajamieh, “Probing Scalar and Pseudoscalar Solutions of the $g - 2$ Anomaly,” *Adv. High Energy Phys.* **2020** (2020) 1751534, [arXiv:1810.08891 \[hep-ph\]](https://arxiv.org/abs/1810.08891).
- [28] M. Bauer, M. Neubert, S. Renner, M. Schnubel, and A. Thamm, “Axionlike Particles, Lepton-Flavor Violation, and a New Explanation of a_μ and a_e ,” *Phys. Rev. Lett.* **124** no. 21, (2020) 211803, [arXiv:1908.00008 \[hep-ph\]](https://arxiv.org/abs/1908.00008).
- [29] C. Cornella, P. Paradisi, and O. Sumensari, “Hunting for ALPs with Lepton Flavor Violation,” *JHEP* **01** (2020) 158, [arXiv:1911.06279 \[hep-ph\]](https://arxiv.org/abs/1911.06279).

[30] D. Kirpichnikov, V. E. Lyubovitskij, and A. S. Zhevlakov, “Constraints on CP-odd ALP couplings from EDM limits of fermions,” [arXiv:2004.13656](https://arxiv.org/abs/2004.13656) [hep-ph].

[31] A. J. Krasznahorkay *et al.*, “Observation of Anomalous Internal Pair Creation in ^{8}Be : A Possible Indication of a Light, Neutral Boson,” *Phys. Rev. Lett.* **116** no. 4, (2016) 042501, [arXiv:1504.01527](https://arxiv.org/abs/1504.01527) [nucl-ex].

[32] A. Krasznahorkay *et al.*, “New experimental results for the 17 MeV particle created in ^{8}Be ,” *EPJ Web Conf.* **137** (2017) 08010.

[33] A. Krasznahorkay *et al.*, “New evidence supporting the existence of the hypothetic X17 particle,” [arXiv:1910.10459](https://arxiv.org/abs/1910.10459) [nucl-ex].

[34] D. Firak *et al.*, “Confirmation of the existence of the X17 particle,” *EPJ Web Conf.* **232** (2020) 04005.

[35] U. Ellwanger and S. Moretti, “Possible Explanation of the Electron Positron Anomaly at 17 MeV in ^{8}Be Transitions Through a Light Pseudoscalar,” *JHEP* **11** (2016) 039, [arXiv:1609.01669](https://arxiv.org/abs/1609.01669) [hep-ph].

[36] J. L. Feng, B. Fornal, I. Galon, S. Gardner, J. Smolinsky, T. M. P. Tait, and P. Tanedo, “Particle physics models for the 17 MeV anomaly in beryllium nuclear decays,” *Phys. Rev. D* **95** no. 3, (2017) 035017, [arXiv:1608.03591](https://arxiv.org/abs/1608.03591) [hep-ph].

[37] J. Hewett *et al.*, “Fundamental Physics at the Intensity Frontier,” 5, 2012. [arXiv:1205.2671](https://arxiv.org/abs/1205.2671) [hep-ex].

[38] R. Essig *et al.*, “Working Group Report: New Light Weakly Coupled Particles,” in *Proceedings, 2013 Community Summer Study on the Future of U.S. Particle Physics: Snowmass on the Mississippi (CSS2013): Minneapolis, MN, USA, July 29-August 6, 2013*. 2013. [arXiv:1311.0029](https://arxiv.org/abs/1311.0029) [hep-ph]. <http://www.slac.stanford.edu/econfs/C1307292/docs/IntensityFrontier/NewLight-17.pdf>.

[39] B. Batell, M. Pospelov, and A. Ritz, “Exploring Portals to a Hidden Sector Through Fixed Targets,” *Phys. Rev. D* **80** (2009) 095024, [arXiv:0906.5614](https://arxiv.org/abs/0906.5614) [hep-ph].

[40] **DELPHI** Collaboration, J. Abdallah *et al.*, “Search for one large extra dimension with the DELPHI detector at LEP,” *Eur. Phys. J. C* **60** (2009) 17–23, [arXiv:0901.4486](https://arxiv.org/abs/0901.4486) [hep-ex].

[41] **BaBar** Collaboration, J. Lees *et al.*, “Search for Invisible Decays of a Dark Photon Produced in $e^{+}e^{-}$ Collisions at BaBar,” *Phys. Rev. Lett.* **119** no. 13, (2017) 131804, [arXiv:1702.03327](https://arxiv.org/abs/1702.03327) [hep-ex].

[42] **NA64** Collaboration, D. Banerjee *et al.*, “Search for Axionlike and Scalar Particles with the NA64 Experiment,” *Phys. Rev. Lett.* **125** no. 8, (2020) 081801, [arXiv:2005.02710](https://arxiv.org/abs/2005.02710) [hep-ex].

[43] **Belle-II** Collaboration, W. Altmannshofer *et al.*, “The Belle II Physics Book,” *PTEP* **2019** no. 12, (2019) 123C01, [arXiv:1808.10567](https://arxiv.org/abs/1808.10567) [hep-ex]. [Erratum: PTEP 2020, 029201 (2020)].

[44] J. Bjorken, S. Ecklund, W. Nelson, A. Abashian, C. Church, B. Lu, L. Mo, T. Nunamaker, and P. Rassmann, “Search for Neutral Metastable Penetrating Particles Produced in the SLAC Beam Dump,” *Phys. Rev. D* **38** (1988) 3375.

[45] M. Raggi and V. Kozhuharov, “Proposal to Search for a Dark Photon in Positron on Target Collisions at DAΦNE Linac,” *Adv. High Energy Phys.* **2014** (2014) 959802, [arXiv:1403.3041 \[physics.ins-det\]](https://arxiv.org/abs/1403.3041).

[46] M. Raggi, V. Kozhuharov, and P. Valente, “The PADME experiment at LNF,” *EPJ Web Conf.* **96** (2015) 01025, [arXiv:1501.01867 \[hep-ex\]](https://arxiv.org/abs/1501.01867).

[47] P. Valente, “POSEYDON - Converting the DAΦNE Collider into a double Positron Facility: a High Duty-Cycle pulse stretcher and a storage ring,” [arXiv:1711.06877 \[physics.acc-ph\]](https://arxiv.org/abs/1711.06877).

[48] P. F. Depta, M. Hufnagel, and K. Schmidt-Hoberg, “Updated BBN constraints on electromagnetic decays of MeV-scale particles,” [arXiv:2011.06519 \[hep-ph\]](https://arxiv.org/abs/2011.06519).

[49] Y. Nomura and J. Thaler, “Dark Matter through the Axion Portal,” *Phys. Rev. D* **79** (2009) 075008, [arXiv:0810.5397 \[hep-ph\]](https://arxiv.org/abs/0810.5397).

[50] M. J. Dolan, F. Kahlhoefer, C. McCabe, and K. Schmidt-Hoberg, “A taste of dark matter: Flavour constraints on pseudoscalar mediators,” *JHEP* **03** (2015) 171, [arXiv:1412.5174 \[hep-ph\]](https://arxiv.org/abs/1412.5174). [Erratum: JHEP 07, 103 (2015)].

[51] T. R. Slatyer, “Indirect dark matter signatures in the cosmic dark ages. I. Generalizing the bound on s-wave dark matter annihilation from Planck results,” *Phys. Rev. D* **93** no. 2, (2016) 023527, [arXiv:1506.03811 \[hep-ph\]](https://arxiv.org/abs/1506.03811).

[52] **Planck** Collaboration, N. Aghanim *et al.*, “Planck 2018 results. VI. Cosmological parameters,” [arXiv:1807.06209 \[astro-ph.CO\]](https://arxiv.org/abs/1807.06209).

[53] **Fermi-LAT** Collaboration, M. Ackermann *et al.*, “Updated search for spectral lines from Galactic dark matter interactions with pass 8 data from the Fermi Large Area Telescope,” *Phys. Rev. D* **91** no. 12, (2015) 122002, [arXiv:1506.00013 \[astro-ph.HE\]](https://arxiv.org/abs/1506.00013).

[54] M. Pospelov, A. Ritz, and M. B. Voloshin, “Secluded WIMP Dark Matter,” *Phys. Lett. B* **662** (2008) 53–61, [arXiv:0711.4866 \[hep-ph\]](https://arxiv.org/abs/0711.4866).

[55] L. Darmé, S. Rao, and L. Roszkowski, “Signatures of dark Higgs boson in light fermionic dark matter scenarios,” *JHEP* **12** (2018) 014, [arXiv:1807.10314 \[hep-ph\]](https://arxiv.org/abs/1807.10314).

[56] L. Darmé, S. Rao, and L. Roszkowski, “Light dark Higgs boson in minimal sub-GeV dark matter scenarios,” *JHEP* **03** (2018) 084, [arXiv:1710.08430 \[hep-ph\]](https://arxiv.org/abs/1710.08430).

[57] G. Krnjaic, “Probing Light Thermal Dark-Matter With a Higgs Portal Mediator,” *Phys. Rev. D* **94** no. 7, (2016) 073009, [arXiv:1512.04119 \[hep-ph\]](https://arxiv.org/abs/1512.04119).

[58] J. A. Evans, A. Ghalsasi, S. Gori, M. Tammaro, and J. Zupan, “Light Dark Matter from Entropy Dilution,” *JHEP* **02** (2020) 151, [arXiv:1910.06319 \[hep-ph\]](https://arxiv.org/abs/1910.06319).

[59] S. Dimopoulos, R. Esmailzadeh, L. J. Hall, and N. Tetradis, “Electroweak phase transition and dark matter abundance,” *Phys. Lett. B* **247** (1990) 601–606.

[60] T. Cohen, D. E. Morrissey, and A. Pierce, “Changes in Dark Matter Properties After Freeze-Out,” *Phys. Rev. D* **78** (2008) 111701, [arXiv:0808.3994 \[hep-ph\]](https://arxiv.org/abs/0808.3994).

[61] J. Jaeckel, P. Malta, and J. Redondo, “Decay photons from the axionlike particles burst of type II supernovae,” *Phys. Rev. D* **98** no. 5, (2018) 055032, [arXiv:1702.02964 \[hep-ph\]](https://arxiv.org/abs/1702.02964).

[62] G. G. Raffelt, “Astrophysical axion bounds,” *Lect. Notes Phys.* **741** (2008) 51–71, [arXiv:hep-ph/0611350](https://arxiv.org/abs/hep-ph/0611350).

[63] G. Lucente, P. Carenza, T. Fischer, M. Giannotti, and A. Mirizzi, “Heavy axion-like particles and core-collapse supernovae: constraints and impact on the explosion mechanism,” [arXiv:2008.04918 \[hep-ph\]](https://arxiv.org/abs/2008.04918).

[64] J. H. Chang, R. Essig, and S. D. McDermott, “Supernova 1987A Constraints on Sub-GeV Dark Sectors, Millicharged Particles, the QCD Axion, and an Axion-like Particle,” *JHEP* **09** (2018) 051, [arXiv:1803.00993 \[hep-ph\]](https://arxiv.org/abs/1803.00993).

[65] W. DeRocco, P. W. Graham, D. Kasen, G. Marques-Tavares, and S. Rajendran, “Supernova signals of light dark matter,” *Phys. Rev. D* **100** no. 7, (2019) 075018, [arXiv:1905.09284 \[hep-ph\]](https://arxiv.org/abs/1905.09284).

[66] F. D’Eramo, N. Fernandez, and S. Profumo, “Dark Matter Freeze-in Production in Fast-Expanding Universes,” *JCAP* **02** (2018) 046, [arXiv:1712.07453 \[hep-ph\]](https://arxiv.org/abs/1712.07453).

[67] A. Sung, H. Tu, and M.-R. Wu, “New constraint from supernova explosions on light particles beyond the Standard Model,” *Phys. Rev. D* **99** no. 12, (2019) 121305, [arXiv:1903.07923 \[hep-ph\]](https://arxiv.org/abs/1903.07923).

[68] J. B. Dent, B. Dutta, D. Kim, S. Liao, R. Mahapatra, K. Sinha, and A. Thompson, “New Directions for Axion Searches via Scattering at Reactor Neutrino Experiments,” *Phys. Rev. Lett.* **124** no. 21, (2020) 211804, [arXiv:1912.05733 \[hep-ph\]](https://arxiv.org/abs/1912.05733).

[69] Y.-S. Tsai, “AXION BREMSSTRAHLUNG BY AN ELECTRON BEAM,” *Phys. Rev. D* **34** (1986) 1326.

[70] J. D. Bjorken, R. Essig, P. Schuster, and N. Toro, “New Fixed-Target Experiments to Search for Dark Gauge Forces,” *Phys. Rev. D* **80** (2009) 075018, [arXiv:0906.0580 \[hep-ph\]](https://arxiv.org/abs/0906.0580).

[71] K. Jodłowski, F. Kling, L. Roszkowski, and S. Trojanowski, “Extending the reach of FASER, MATHUSLA, and SHiP towards smaller lifetimes using secondary particle production,” *Phys. Rev. D* **101** no. 9, (2020) 095020, [arXiv:1911.11346 \[hep-ph\]](https://arxiv.org/abs/1911.11346).

[72] A. Celentano, L. Darmé, L. Marsicano, and E. Nardi, “New production channels for light dark matter in hadronic showers,” [arXiv:2006.09419 \[hep-ph\]](https://arxiv.org/abs/2006.09419).

[73] Y.-S. Tsai and V. Whitis, “THICK TARGET BREMSSTRAHLUNG AND TARGET CONSIDERATION FOR SECONDARY PARTICLE PRODUCTION BY ELECTRONS,” *Phys. Rev.* **149** (1966) 1248–1257.

[74] J. Jaeckel and M. Spannowsky, “Probing MeV to 90 GeV axion-like particles with LEP and LHC,” *Phys. Lett. B* **753** (2016) 482–487, [arXiv:1509.00476 \[hep-ph\]](https://arxiv.org/abs/1509.00476).

[75] P. J. Fox, R. Harnik, J. Kopp, and Y. Tsai, “LEP Shines Light on Dark Matter,” *Phys. Rev. D* **84** (2011) 014028, [arXiv:1103.0240 \[hep-ph\]](https://arxiv.org/abs/1103.0240).

[76] A. Belyaev, N. D. Christensen, and A. Pukhov, “CalcHEP 3.4 for collider physics within and beyond the Standard Model,” *Comput. Phys. Commun.* **184** (2013) 1729–1769, [arXiv:1207.6082 \[hep-ph\]](https://arxiv.org/abs/1207.6082).

[77] **DELPHI** Collaboration, J. Abdallah *et al.*, “Photon events with missing energy in e+ e- collisions at $s^{**}(1/2) = 130\text{-GeV}$ to 209-GeV,” *Eur. Phys. J. C* **38** (2005) 395–411, [arXiv:hep-ex/0406019](https://arxiv.org/abs/hep-ex/0406019).

[78] R. Brun and F. Rademakers, “ROOT: An object oriented data analysis framework,” *Nucl. Instrum. Meth. A* **389** (1997) 81–86.

[79] E. Riordan *et al.*, “A Search for Short Lived Axions in an Electron Beam Dump Experiment,” *Phys. Rev. Lett.* **59** (1987) 755.

[80] B. Batell, R. Essig, and Z. Surujon, “Strong Constraints on Sub-GeV Dark Sectors from SLAC Beam Dump E137,” *Phys. Rev. Lett.* **113** no. 17, (2014) 171802, [arXiv:1406.2698 \[hep-ph\]](https://arxiv.org/abs/1406.2698).

[81] L. Marsicano, M. Battaglieri, M. Bondi’, C. R. Carvajal, A. Celentano, M. De Napoli, R. De Vita, E. Nardi, M. Raggi, and P. Valente, “Dark photon production through positron annihilation in beam-dump experiments,” *Phys. Rev. D* **98** no. 1, (2018) 015031, [arXiv:1802.03794 \[hep-ex\]](https://arxiv.org/abs/1802.03794).

[82] **PADME** Collaboration, G. Piperno, “First results on the performance of the PADME electromagnetic calorimeter,” *JINST* **15** no. 05, (2020) C05008, [arXiv:2002.11671 \[physics.ins-det\]](https://arxiv.org/abs/2002.11671).

[83] **Muon g-2** Collaboration, G. Bennett *et al.*, “Final Report of the Muon E821 Anomalous Magnetic Moment Measurement at BNL,” *Phys. Rev. D* **73** (2006) 072003, [arXiv:hep-ex/0602035](https://arxiv.org/abs/hep-ex/0602035).

[84] T. Aoyama *et al.*, “The anomalous magnetic moment of the muon in the Standard Model,” [arXiv:2006.04822 \[hep-ph\]](https://arxiv.org/abs/2006.04822).

[85] R. H. Parker, C. Yu, W. Zhong, B. Estey, and H. Müller, “Measurement of the fine-structure constant as a test of the Standard Model,” *Science* **360** (2018) 191, [arXiv:1812.04130 \[physics.atom-ph\]](https://arxiv.org/abs/1812.04130).

[86] T. Aoyama, T. Kinoshita, and M. Nio, “Revised and Improved Value of the QED Tenth-Order Electron Anomalous Magnetic Moment,” *Phys. Rev. D* **97** no. 3, (2018) 036001, [arXiv:1712.06060 \[hep-ph\]](https://arxiv.org/abs/1712.06060).

[87] J. P. Leveille, “The Second Order Weak Correction to $(g-2)$ of the Muon in Arbitrary Gauge Models,” *Nucl. Phys. B* **137** (1978) 63–76.

[88] L. Darmé, L. Di Luzio, M. Giannotti, and E. Nardi, “Selective enhancement of the QCD axion couplings,” [arXiv:2010.15846 \[hep-ph\]](https://arxiv.org/abs/2010.15846).

[89] F. Björkeroth, E. J. Chun, and S. F. King, “Flavourful Axion Phenomenology,” *JHEP* **08** (2018) 117, [arXiv:1806.00660 \[hep-ph\]](https://arxiv.org/abs/1806.00660).

[90] L. Marsicano, M. Battaglieri, A. Celentano, R. De Vita, and Y.-M. Zhong, “Probing Leptophilic Dark Sectors at Electron Beam-Dump Facilities,” *Phys. Rev. D* **98** no. 11, (2018) 115022, [arXiv:1812.03829 \[hep-ex\]](https://arxiv.org/abs/1812.03829).

[91] C.-Y. Chen, J. Kozaczuk, and Y.-M. Zhong, “Exploring leptophilic dark matter with NA64- μ ,” *JHEP* **10** (2018) 154, [arXiv:1807.03790 \[hep-ph\]](https://arxiv.org/abs/1807.03790).

[92] Y. Kahn, G. Krnjaic, N. Tran, and A. Whitbeck, “M³: a new muon missing momentum experiment to probe $(g-2)_\mu$ and dark matter at Fermilab,” *JHEP* **09** (2018) 153, [arXiv:1804.03144 \[hep-ph\]](https://arxiv.org/abs/1804.03144).

[93] **Belle II** Collaboration, I. Adachi *et al.*, “Search for an Invisibly Decaying Z' Boson at Belle II in $e^+e^- \rightarrow \mu^+\mu^-(e^\pm\mu^\mp)$ Plus Missing Energy Final States,” *Phys. Rev. Lett.* **124** no. 14, (2020) 141801, [arXiv:1912.11276 \[hep-ex\]](https://arxiv.org/abs/1912.11276).